

Complementary Use of Glider Data, Altimetry, and Model for Exploring Mesoscale Eddies in the Tropical Pacific Solomon Sea

L. Gourdeau, J. Verron, Alexis Chaigneau, S. Cravatte, W. Kessler

▶ **To cite this version:**

L. Gourdeau, J. Verron, Alexis Chaigneau, S. Cravatte, W. Kessler. Complementary Use of Glider Data, Altimetry, and Model for Exploring Mesoscale Eddies in the Tropical Pacific Solomon Sea. Journal of Geophysical Research. Oceans, 2017, 122, pp.9209-9229. 10.1002/2017JC013116 . insu-03706518

HAL Id: insu-03706518

https://insu.hal.science/insu-03706518

Submitted on 28 Jun 2022

HAL is a multi-disciplinary open access archive for the deposit and dissemination of scientific research documents, whether they are published or not. The documents may come from teaching and research institutions in France or abroad, or from public or private research centers.

L'archive ouverte pluridisciplinaire **HAL**, est destinée au dépôt et à la diffusion de documents scientifiques de niveau recherche, publiés ou non, émanant des établissements d'enseignement et de recherche français ou étrangers, des laboratoires publics ou privés.

Copyright

AGU PUBLICATIONS

JGR

Journal of Geophysical Research: Oceans

RESEARCH ARTICLE

10.1002/2017JC013116

Complementary Use of Glider Data, Altimetry, and Model for Exploring Mesoscale Eddies in the Tropical Pacific Solomon Sea

L. Gourdeau[1], J. Verron[2], A. Chaigneau[1], S. Cravatte[1], and W. Kessler[3]

[1]LEGOS, Université de Toulouse, CNES, CNRS, IRD, UPS, Toulouse, France, [2]IGE, CNRS, IRD, , Université Grenoble Alpes, Grenoble, France, [3]NOAA/Pacific Marine Environmental Laboratory, Seattle, WA, USA

Key Points:
- These tropical eddies have a limited depth extension (from the surface to 150/180 m depth)
- Model, glider, and satellite data are consistent and provide complementary information
- Temperature and salinity eddy signatures suggest that eddies could be particularly efficient in diapycnal and isopycnal mixing

Correspondence to:
L. Gourdeau,
lionel.gourdeau@legos.obs-mip.fr

Citation:
Gourdeau, L., Verron, J., Chaigneau, A., Cravatte, S., & Kessler, W. (2017). Complementary use of glider data, altimetry, and model for exploring mesoscale eddies in the tropical Pacific Solomon Sea. *Journal of Geophysical Research: Oceans*, *122*, 9209–9229. https://doi.org/10.1002/2017JC013116

Received 24 MAY 2017
Accepted 5 NOV 2017
Accepted article online 10 NOV 2017
Published online 29 NOV 2017

© 2017. American Geophysical Union. All Rights Reserved.

Abstract Mesoscale activity is an important component of the Solomon Sea circulation that interacts with the energetic low-latitude western boundary currents of the South Tropical Pacific Ocean carrying waters of subtropical origin before joining the equatorial Pacific. Mixing associated with mesoscale activity could explain water mass transformation observed in the Solomon Sea that likely impacts El Niño Southern Oscillation dynamics. This study makes synergetic use of glider data, altimetry, and high-resolution model for exploring mesoscale eddies, especially their vertical structures, and their role on the Solomon Sea circulation. The description of individual eddies observed by altimetry and gliders provides the first elements to characterize the 3-D structure of these tropical eddies, and confirms the usefulness of the model to access a more universal view of such eddies. Mesoscale eddies appear to have a vertical extension limited to the Surface Waters (SW) and the Upper Thermocline Water (UTW), i.e., the first 140–150 m depth. Most of the eddies are nonlinear, meaning that eddies can trap and transport water properties. But they weakly interact with the deep New Guinea Coastal Undercurrent that is a key piece of the equatorial circulation. Anticyclonic eddies are particularly efficient to advect salty and warm SW coming from the intrusion of equatorial Pacific waters at Solomon Strait, and to impact the characteristics of the New Guinea Coastal Current. Cyclonic eddies are particularly efficient to transport South Pacific Tropical Water (SPTW) anomalies from the North Vanuatu Jet and to erode by diapycnal mixing the high SPTW salinity.

1. Introduction

The Solomon Sea located north of the Coral Sea in the tropical South West Pacific is a key pathway connecting the subtropics to the equator through the Low-Latitude Western Boundary Currents (LLWBCs; Figure 1a). Understanding the large-scale circulation of this region and its variability is one of the main issues of the CLIVAR/Southwest Pacific Ocean and Climate Experiment (SPICE, Ganachaud et al., 2014). Part of the waters transiting through the Solomon Sea feed the equatorial current system, in particular the Equatorial Undercurrent (EUC) (e.g., Grenier et al., 2011, Qin et al., 2015), and ultimately the equatorial cold tongue; the physical and biogeochemical properties of the waters are potentially modified during their transit of this Sea (Grenier et al., 2013), making these processes important for the downstream circulation. The goal of the present work is to examine one mechanism that could produce such modification.

The circulation in this semienclosed basin has been described in numerous studies, from observations, and model outputs (Cravatte et al., 2011; Davis et al., 2012; Djath et al., 2014a; Gasparin et al., 2012; Germineaud et al., 2016; Hristova & Kessler, 2012; Melet et al., 2010a, 2010b). It is highly constrained by bathymetric features (Figure 1b). A strong LLWBC, the New Guinea Coastal Undercurrent (NGCU) flows from the southern entrance of the Solomon Sea along the Papua New Guinea (PNG) coast. When approaching the New Britain coast, it separates into two branches that exit the Solomon Sea through Vitiaz and Solomon Straits and St. George's Channel. The NGCU flows at the thermocline level below highly variable surface currents including the New Guinea Coastal Current (NGCC), and the Solomon Strait Inflow (SSI) that is the part of the South Equatorial Current (SEC) entering the Solomon Sea through Solomon Strait (Hristova & Kessler, 2012; Melet et al., 2010a).

The Solomon Sea is an area of high eddy kinetic energy (EKE), and surface mesoscale vortices have been studied by a complementary approach using a numerical model and altimetric data (Gourdeau et al., 2014).

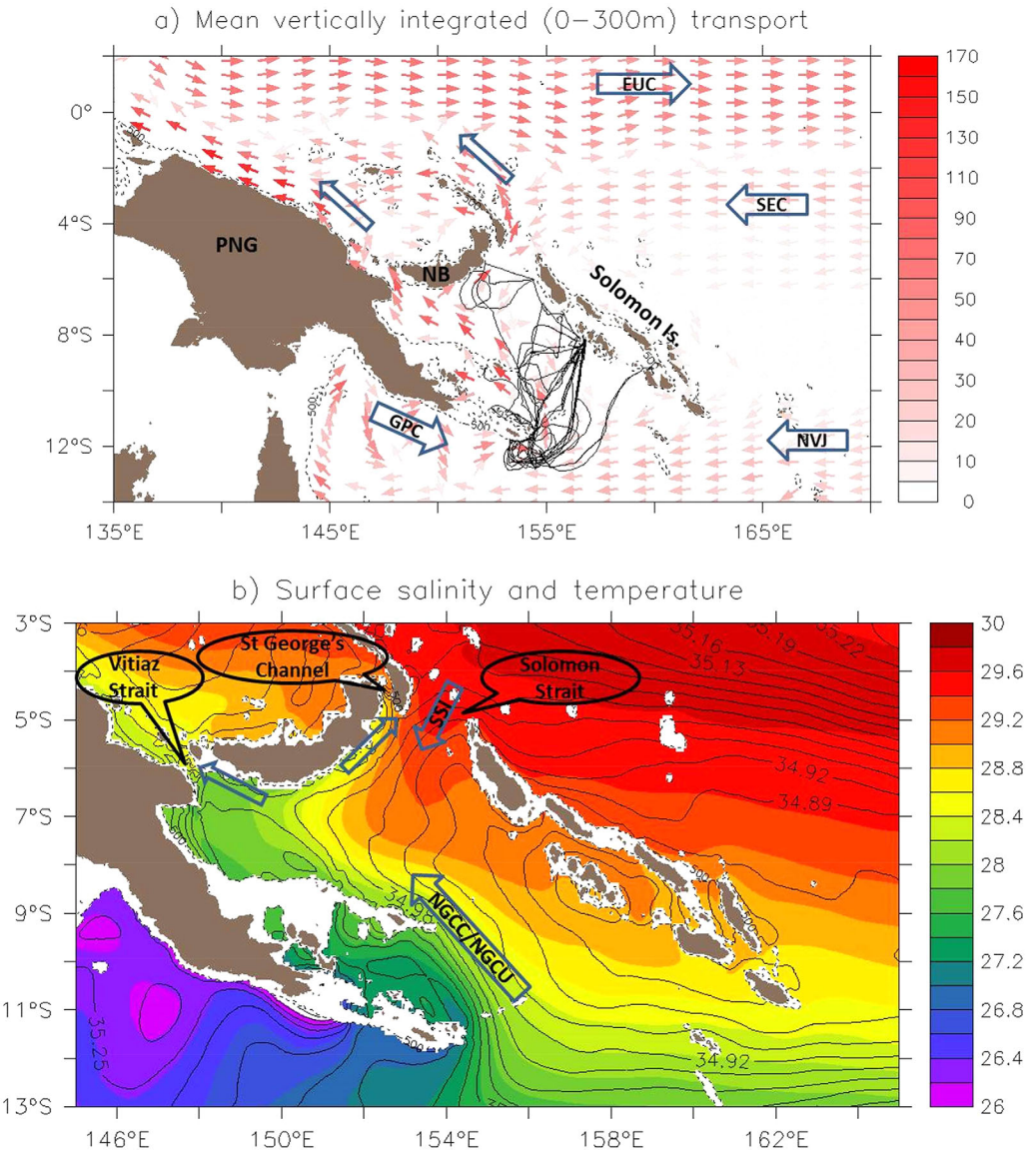


Figure 1. (a) Mean vertically integrated (0–300 m) transport (in $m^2\ s^{-1}$) in the southwestern tropical Pacific computed from the Drakkar ORCA12 simulation. Superimposed are the 11 glider tracks sampling the Solomon Sea circulation during the 2007–2011 period. The main currents surrounding the Solomon Sea are shown in Figure 1a: the Gulf of Papua Current (GPC), the North Vanuatu Jet (NVJ), the South Equatorial Current (SEC), and the Equatorial Undercurrent (EUC). PNG stands for Papua New Guinea and NB for New Britain. (b) A zoom in on the Solomon Sea of the mean sea-surface salinity (SSS in contours) and temperature (SST in color, °C) from the Drakkar ORCA12 simulation. Arrows stand for the main Solomon Sea currents which are the New Guinea Coastal Current (NGCC), New Guinea Coastal Undercurrent (NGCU), and the Solomon Strait Inflow (SSI). The dashed line represents the 500 m isobath. Additional arrows in Figures 1a and 1b show direction of mean flow.

In this study, mesoscale activity in the Solomon Sea was found to be mainly generated by instabilities of the regional large-scale currents, and their modulation at seasonal and interannual timescales to be highly related to the intrusion of the SSI that modulates the vertical and horizontal shears suitable for instabilities. As an illustration, during El Niño events the LLWBCs are stronger but the mesoscale activity decreases associated with a weaker SSI. The opposite situation prevails during La Niña events during which the mesoscale activity is enhanced. Another study based on numerical modeling has also shown that large mesoscale eddies, having radii larger than 80 km, are generated by mixed barotropic/baroclinic instabilities of the near-boundary surface flow, and account for most of the surface EKE and its annual modulation (Hristova

et al., 2014). At depth in the thermocline and intermediate levels, the EKE in the Solomon Sea is dominated by the LLWBC variability at short spatial scales.

As part of the Consortium on the Ocean's Role in Climate (CORC) program on boundary current, Spray gliders have been routinely deployed at the Solomon Sea entrance since 2007, mainly to monitor the transports entering the Solomon Sea and the characteristics and distribution of water masses (Davis et al., 2012). The volume transport variability is well correlated with El Niño indices, but the glider time series include O(3 Sv) noise from transient eddies not well sampled by the slowly moving glider. The eddy signatures appear as fluctuations of depth-averaged velocities with typical values of 0 (10 cm s^{-1}) and spatial scales of 100–200 km.

The Solomon Sea exhibits spatial variations of background temperature and salinity that characterize different water origins from the North Vanuatu Jet (NVJ), the Gulf of Papua Current (GPC), and the SSI (Figure 1b). Therefore, eddies traveling in the Solomon Sea could contribute to mixing these different water masses. Despite their potential role on water mass characteristics and their interaction with LLWBCs that may impact the large scale circulation (Melet et al., 2011, 2012), the characteristics of mesoscale eddies in the Solomon Sea have not been fully explored.

This study combines glider data, altimetry, and model to investigate Solomon Sea eddies. Altimetric maps are used to detect mesoscale eddies that have a signature on sea level, whereas glider data provide the vertical structure of some detected eddies. The model validated against observations, is used to get a synoptic view of the mesoscale eddies in the Solomon Sea. The objective of this paper is thus to extend the works of Gourdeau et al. (2014) and Hristova et al. (2014) by investigating the vertical structure of the Solomon Sea eddies in order to get new insights on their role on the Solomon Sea circulation and mixing, and possibly on basin-scale circulations.

The paper is organized as follows. In section 2, the different data sets used in this study are described with a focus on the eddy-tracking algorithm, and a cross validation of absolute geostrophic current from gliders and altimetry. Section 3 describes the few eddies sampled by gliders observations. Their along-track signatures are compared with those simulated by the model. Section 4 focuses on modeled eddies by providing synoptic analyses of eddy anomalies, and their consequences on water masses and Solomon Sea circulation.

2. Data, Model, and Eddy Identification

In this section, the different data sets used are presented. A comparison between altimetry and glider data confirms the potential to jointly use the two complementary data sets. An eddy detection and tracking tool is applied both to altimetric dynamic topography and modeled sea surface height fields. The resulting eddy database is used to explore individual in situ eddies (section 3), and to get a synoptic view of eddies (section 4).

2.1. Gliders

Since 2007, Spray gliders (Sherman et al., 2001) have operated 3–4 missions per year in the Solomon Sea. Eleven missions are considered for this study covering the November 2007 to January 2011 period (Table 1). Transects are made between the Solomon Islands and the southeastern tip of Papua New Guinea (Figure 1a). A round trip across the Solomon Sea may take up to 5 months, and successive transects usually overlap. Most of the transects consist of sequential dives down to 700 m depth, except for three early transects with gliders diving only to 500–600 m depth.

Temperature and salinity profiles were collected using a Seabird CP41 CTD during every ascent of the glider, which are typically spaced 4 km and 4 h apart. With 4 h sampling, glider data partly resolve tidal signals that can therefore be filtered out (Gourdeau et al., 2008). Data have been smoothed using a triangle filter with half power at 30 km to filter out small-scale oscillation due to internal waves. Geostrophic velocity shears derived from the temperature/salinity data through the thermal wind equations are referenced to depth-averaged absolute currents to get the cross-track absolute geostrophic velocities (e.g., Davis et al., 2012; Gourdeau et al., 2008; Pietri et al., 2014). The depth-averaged absolute current is derived from the difference between vehicle motion as measured by GPS fixes and the actual distance traveled through the water. Through-water speed is computed from the vertical velocity (deduced from pressure changes),

Table 1
Glider Mission

	1	2	3	4	5	6
	14/11/2007	27/02/2008	04/07/2008	10/11/2008	13/07/2009	13/07/2009
Mission	04/02/2008	18/07/2008	15/10/2008	01/02/2009	01/11/2009	31/10/2009
UgeoAbs/DT	0.83	0.68	0.64	0.79	0.59	0.76
Eddies	1SC 3PC 4A	2PC 4A	1SC 3PC 1A	1SC 3PC 2A	2SC 2PC	2SC 2PC
ENSO	Niña	Niña	Neutral	Neutral	Niño	Niño
Eddies glider	0	**1A**	0	**1PC**	0	0

Mission	7	8	9	10	11
	7/11/2009	19/04/2010	19/04/2010	28/09/2010	31/01/2011
	24/02/2010		09/09/2010	24/01/2011	31/05/2011
UgeoAbs/DT	0.70	0.76	0.70	0.67	0.77
Eddies	2SC 2PC	1SC 4PC 1A	3SC 3PC 2A	4PC 3A	2PC 3A
ENSO	Niño	Neutral	Neutral	Niña	Niña
Eddies glider	0	2C	**1SC**	1C	1A

Note. For every glider mission, the first row is the correlation between the absolute geostrophic velocity from altimetry and the cross-track absolute geostrophic velocity from the glider averaged in the 0–150 m depth (UgeoAbs/DT). The second row exhibits the different Solomon Sea eddies observed by altimetry (PC, Propagating Cyclonic eddies; SC, Stationary cyclonic eddies; A, Anticyclonic eddies) during the glider mission to relate to ENSO conditions (third row). The fourth row exhibits eddies observed by the glider. In bold are eddies discussed on section 3.1.

measured vehicle pitch, and a simple model of vehicle dynamics. The reader is referred to Davis et al. (2012) for more details on these data and their processing.

As an example, the glider mission #2 realized between February and July 2008 is shown in Figure 2. This mission started at Guadalcanal (Solomon Islands, Km 0), crossed the southern Solomon Sea, and sampled the NGCU at the southeastern tip of PNG (Km 1,100), before going north until the tip of the Woodlark Archipelago (PNG, Km 1,450), then recrossing the Sea to Gizo (Solomon Islands, Km 1,900). During its round trip the glider traveled 1,900 km and sampled tropical Pacific water characterized by a well-marked thermocline (centered near 20°C) associated with a salinity maximum (>35.6) typical of South Pacific Tropical Waters (SPTW, $\sigma = 24.3 - 25.3$ kg m^{-3}) advected by the NVJ before joining the NGCU in the Solomon Sea (Gasparin et al., 2014; Grenier et al., 2013). The eastern and western parts of the Solomon Sea entrance are well contrasted with a 40 cm difference in dynamic height between the beginning of the glider mission and ~1,100 km further. As discussed in the next section, a fraction of this signal is due to the presence of an anticyclonic eddy offshore Solomon Islands at the beginning of the mission (Km 100–300, see black vertical lines in Figure 2b). The NGCU is well identified on the velocity section in the 950–1,200 km range by currents extending deep in subsurface with positive and negative signatures that trace the route of the LLWBC around the southern tip of PNG. The Eastern Solomon Sea (Km 0–400) is characterized by warm near-surface waters (> 28°C) extending deep (> 150 m depth, Figure 2c), whereas the salinity maximum of the SPTW is more pronounced along the southern entrance of the Solomon Sea (Km 0–1,000) than in the interior of the Solomon Sea where it seems eroded (Km 1,000–1,900) (Figure 2d).

2.2. Altimetry

The altimetric data set comes from the Ssalto/Duacs gridded multimission altimeter product provided in delayed time that is now distributed through the CMEMS data access services (http://www.marine.copernicus.eu). On 2014, this product has been released with several upgrades and delivered on a daily basis and on a 1/4° × 1/4° grid. In this study, we used the former product used in Gourdeau et al. (2014) that covers the November 1992 to December 2011 period. This product ("Merged MSLA-H DT in Global area") combines data from up to four altimetry satellites (Topex/Poseidon, Jason1–2, ERS1–2, or Envisat, and Geosat Follow On), and the mapping procedure based on optimal interpolation was applied to produce weekly maps of Sea Level Anomaly (MSLA) on a 1/3° × 1/3° grid. Both altimetric gridded products are sensitive to the complex geography of the Solomon Sea with its numerous islands that can induce spurious results on the mapping procedure. Indeed, data were often interpolated over islands (such as the New Britain Island or the Solomon Island chain) that separate distinct dynamical regimes. Despite this limitation, the MSLA product

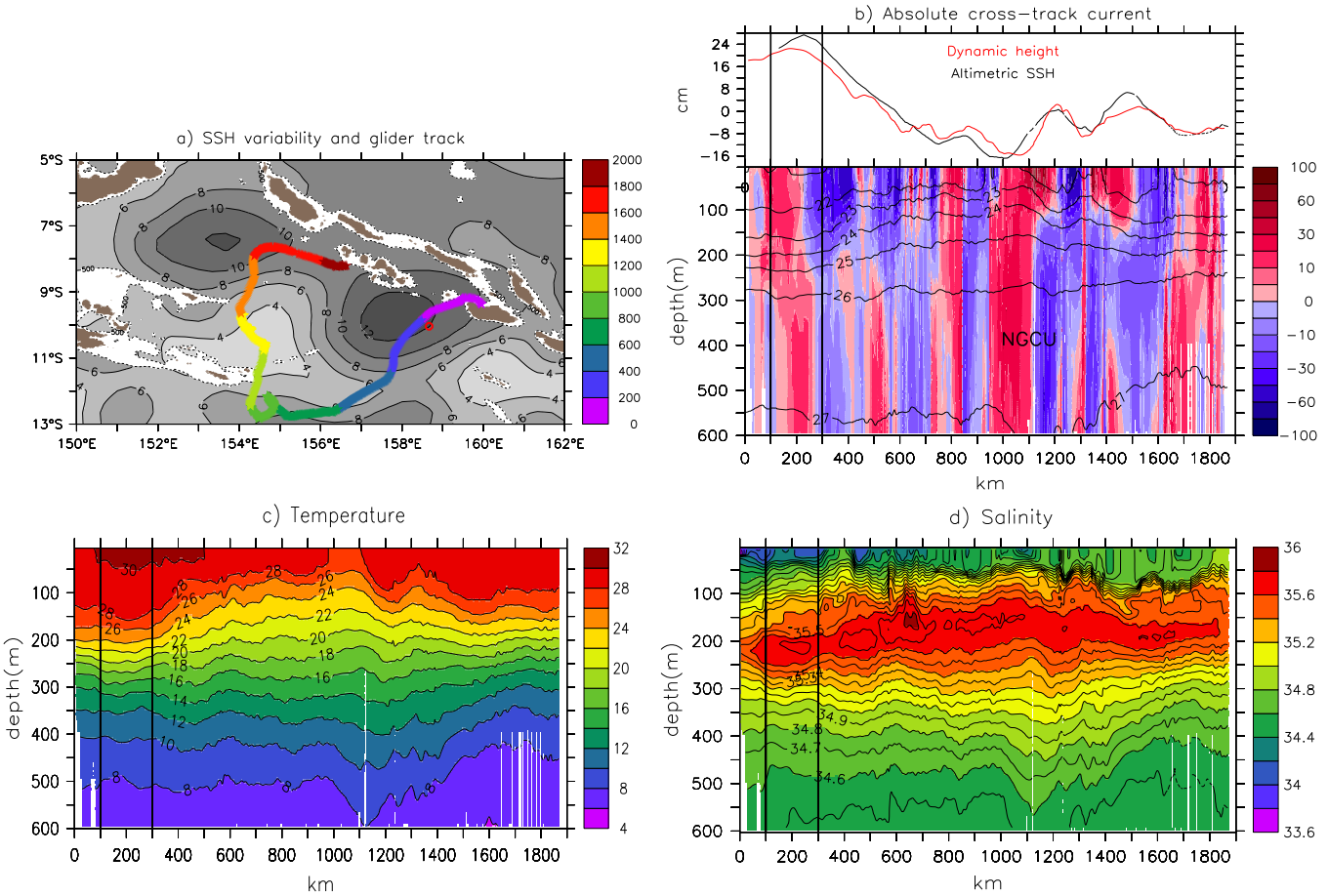


Figure 2. Description of the glider mission #2. (a) Distance (in km, colors) covered from the beginning of the glider's mission. Grey shading shows the standard deviation of SSH (in cm) during the 5 months of the glider mission. (b)–(d) Vertical profiles along the glider track of absolute cross-track geostrophic velocity (cm s^{-1}, positive to the right of the track), temperature (°C), and salinity sampled by the glider, respectively. On top of Figure 2b, are shown the dynamic height inferred from glider data (in red) and the SSH from altimetry (in black), in cm. Thick black lines in Figures 2b–2d delineate the anticyclonic eddy describes in section 3.1.

used here was able to provide useful information to understand the seasonal and interannual current variability in the Solomon Sea (Melet et al., 2010b).

As in Gourdeau et al. (2014), MSLA was referenced to the MDT_CNES-CLS09 mean ocean dynamic topography (Rio et al., 2011) to get absolute measurements of the ocean Dynamic Topography (DT). Using DT instead of MSLA data is beneficial to consistently compare altimetric observations with the absolute information from glider data and from the modeled Sea Surface Height (SSH). Although it is challenging to produce a high-quality mean dynamic topography product in this complex region, it compares well with the time-averaged modeled SSH (not shown), and the DT fields have been successfully used to explore the surface mesoscale activity in the Solomon Sea (Gourdeau et al., 2014).

2.3. Glider/Altimetry Comparisons

Altimetric DT fields were linearly interpolated in time and space to glider trajectories. Glider-measured dynamic height and cross-track absolute near-surface geostrophic velocities compare relatively well with derived altimetric fields as illustrated for mission #2 (Figures 2b and 3). Depending on the missions, spatial correlations vary from 0.59 to 0.83 (Table 1). They are systematically higher when glider velocity data are averaged over the 0–150 m depth (from the surface down to the upper thermocline) than when considering surface glider data only. This is probably due to the different space/time sampling between altimetry and glider. Gliders, with their high-frequency sampling, not only resolve geostrophic dynamics but also ageostrophic dynamics (e.g., mixed layer dynamics, wind-induced dynamics, etc.) that are notably present

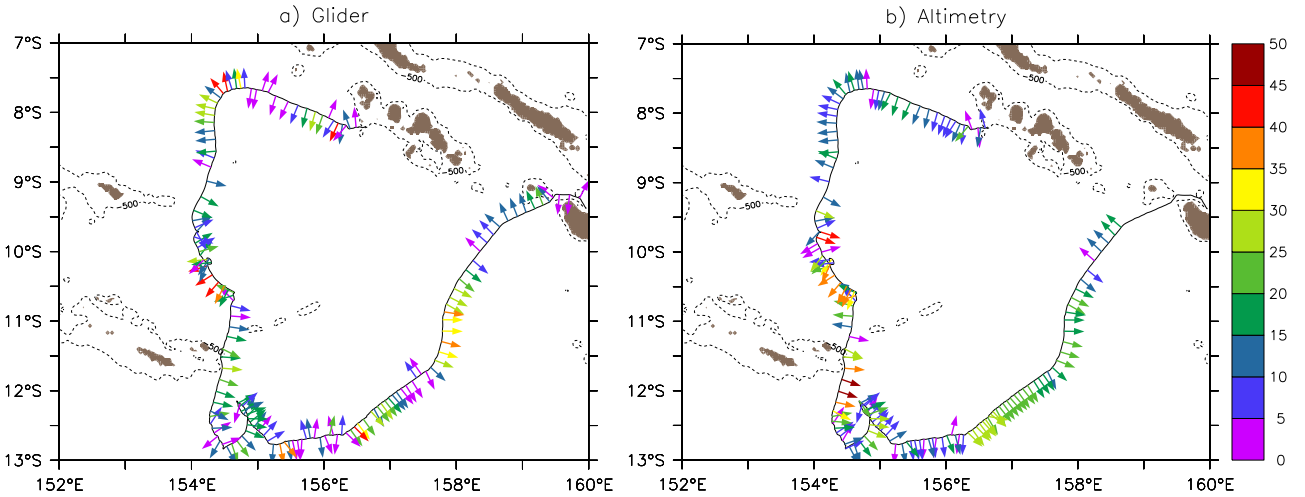


Figure 3. Absolute cross-track geostrophic current (in cm s^{-1}) for the glider mission #2 estimated (a) from glider averaged over the 0–150 m depth and (b) from altimetry.

near the surface. This ageostrophic signal is partly attenuated when averaging in the vertical, increasing the correlation with altimetry. The standard deviation of the glider current averaged over the 0–150 m depth is of similar magnitude than the one from altimetry, about 15–20 cm s^{-1} rms. These comparisons convince us to use altimetric and glider data jointly to detect eddies shared by both data set (section 2.5).

2.4. Model: DRAKKAR 1/12°

The model used is the ORCA12.L46-MAL95 configuration of the global 1/12° OGCM developed and operated in the DRAKKAR consortium (Lecointre et al., 2011). This model is based on OPA, the ocean physical component of the NEMO ocean modeling system (Madec, 2008). NEMO-OPA resolves the classic primitive equations on a sphere, discretized on an Arakawa C grid with a Mercator projection. Geopotential vertical coordinates are used with 46 levels, having a vertical resolution of 6 m in the upper layers and up to 250 m in the deepest regions (5,750 m). The "partial step" approach is used (Adcroft et al., 1997) to allow the bottom cells thickness to be modified to fit the local bathymetry. This approach clearly improves the representation of topography effects (Barnier et al., 2006; Penduff et al., 2007). The bathymetry was built from the GEBCO1 data set for regions shallower than 200 m and from ETOPO2 for regions deeper than 400 m (with a combination of both data sets in the 200–400 m depth range). Lateral boundary conditions for coastal tangential velocity have a strong impact on the stability of boundary currents (Verron & Blayo, 1996). Based on sensitivity experiments, "partial-slip" condition, where the coastal vorticity is not set to 0 ("free slip" condition), but is weaker than in the "no-slip" condition, is chosen. The atmospheric forcing (both mechanical and thermodynamical) is applied to the model using the CORE bulk-formulae approach (Large & Yeager, 2004, 2009).

The simulation started from rest in 1978 with initial conditions for temperature and salinity provided by the 1998 World Ocean Atlas (Levitus, 1998). This is a free run without data assimilation. It was spun up for 11 years using the CORE-II forcing data set and then integrated from 1989 to 2007 using an ERA-interim derived forcing. The 3-D ocean state (temperature, salinity, velocities), and the 2-D Sea Surface Height (SSH) are saved as 5 day means during the period of integration. More details on this simulation and its validation in the Solomon Sea can be found in Djath et al. (2014b).

2.5. Detection and Tracking of Surface Eddies

Coherent mesoscale vortices are algorithmically detected in altimetric DT maps and in modeled SSH fields using the method developed by Chaigneau et al. (2008, 2009). To detect cyclonic eddies (CEs), and anticyclonic eddies (AEs), the algorithm first searches for potential eddy centers by locating a local DT/SSH extremum in a moving window of 1° × 1°. Then, for each potential center, the algorithm looks for closed DT/SSH contours around this extremum with an increment of 10^{-4} m. The outermost closed contour embedding the considered eddy center defines the edge of the eddy. Only eddies having an amplitude higher than

2 cm (absolute difference of DT/SSH from the center to the edge) are considered. For each identified eddy, the equivalent radius (R) corresponds to the radius of an equivalent disk having the same area. In a second step, each eddy is temporally tracked from its appearance to its dissipation. Eddy tracking from one frame to the next one is performed by comparing each eddy of the current time frame with the ones located within a radius of 150 km. The corresponding eddy in the next time frame is then identified from the minimum of the cost function evaluating the mismatch between the distance separating them, vorticity, kinetic energy, and radius (Chaigneau et al., 2008). The trajectories and evolution of eddies in the Solomon Sea, identified by the eddy-tracking algorithm, compose an eddy database that are used in the following analysis.

Such detection and tracking algorithms have already been used in Gourdeau et al. (2014). They have shown the existence of two types of CEs: "propagating" CEs generated in the southern basin and that propagate northwestward (PCEs), and "stationary" CEs located in the northern basin (SCEs). AEs are generated in the eastern part of the Solomon Sea and propagate westward before dissipating in the central Solomon Sea. In this study, to quantify and track robust features, PCEs are defined as eddies generated in the southern Solomon Sea (south of 9°S), and traveling more than 300 km; SCEs are defined as eddies generated in the northern Solomon Sea (north of 9°S), traveling less than 200 km, and having a lifespan higher than 5 weeks; and

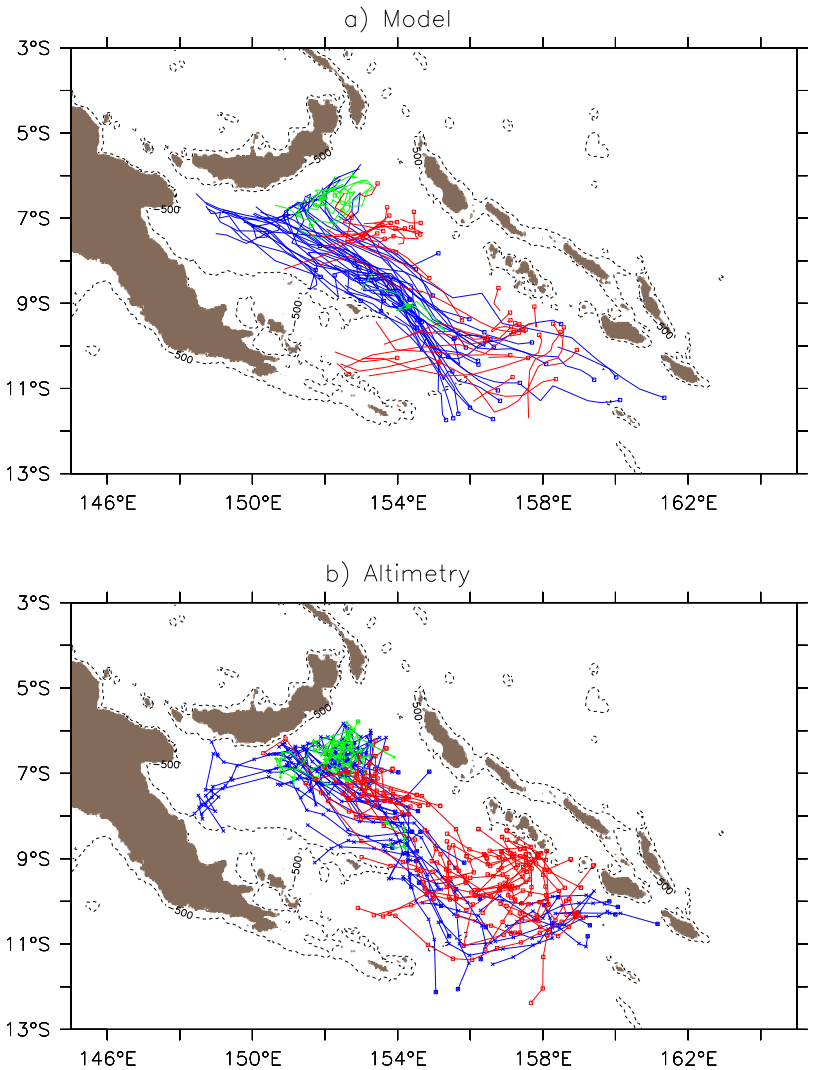


Figure 4. Distribution of the propagating CEs (in blue, defined by propagating distances > 300 km), stationary CEs (in green, defined by a life span > 5 weeks and by propagating distances < 200 km), and AEs (in red) for (a) the model and (b) altimetry.

AEs are defined to travel more than 100 km and to have a lifespan higher than 3 weeks. Based on altimetric DT maps, 194 PCEs, 266 SCEs, and 435 AEs corresponding to 20, 24, and 84 trajectories, respectively, were detected over the 1992–2011 period. Similarly, based on modeled SSH fields, 367 PCEs, 178 SCEs, and 151 AEs corresponding to 33, 15, and 29 trajectories, respectively, have been detected for the 1989–2007 period. Their distribution is presented in Figure 4, and illustrates the relatively good agreement in terms of distribution between model and altimetry.

Compared to SCEs and AEs, PCEs are more numerous in the model than in altimetry. It could be the result of relatively low energetic PCEs, as suggested in the next section that are more difficult to detect in altimetry than in the model. The mean cyclonic circulation present in the northern basin south of New Britain (Figure 1 in Gourdeau et al., 2014), more energetic in the mean DT (Rio et al., 2011) than in the mean modeled SSH (not shown) could explain more numerous SCEs in altimetry than in the model. There are three times more of AEs in altimetry than in the model. As seen in Figure 4, many AEs are detected in altimetry but not in the model in the vicinity of the Solomon Islands. Such significant discrepancy in AEs could be explained both by lower level of EKE in the model than estimated from in situ observation (Gourdeau et al., 2014; Hristova & Kessler, 2012) and by the sensitivity of the modulation of EKE to the number of AEs (Gourdeau et al., 2014). We may expect that a lower level of EKE in the model is a consequence of fewer AEs.

In the next section, results are presented with regard to the different eddy types.

3. Analysis of Individual Eddies Along the Glider Tracks

The eddy database is used to collocate in time and space eddies sampled by the glider. During the 4–5 months period of a typical glider mission, between four and eight eddies are detected from altimetry in the whole Solomon Sea. However, only 7 eddies were sampled by gliders during the 11 glider missions considered in this paper (Table 1): 1 SCE, 4 PCEs, and 2 AEs. Although the few sampled eddies are unable to provide a robust mean vertical structure of eddies in the Solomon Sea, they allow a first description of the different eddy types. In order to define the location of the eddies' centers and edges along the glider tracks, we carefully checked the trajectory of the glider inside the eddies by comparing the altimetric SSH maps with the along-track absolute surface geostrophic velocity (see Figure 5a for an example).

The dynamic height signature of an eddy translates into isopycnal displacements inducing temperature and salinity anomalies at a given depth. Eddy anomaly for a field at a given depth is computed using the "differential anomaly method" (Simpson et al., 1984):

$$\mathrm{Ta}(\mathrm{r},\mathrm{z}) = \mathrm{Te}(\mathrm{r},\ \mathrm{z}) - \mathrm{Tr}(\mathrm{z}), \tag{1}$$

where Te(r, z) is the temperature (salinity) of the eddy at some radial distance r from the eddy center and at depth z. Tr(z) is the reference temperature (salinity) constructed averaging temperature (salinity) profiles outside the eddy (in a 50 km range from its edges) at the corresponding depth.

3.1. Eddy Vertical Structure as Inferred From Glider Observations

As mentioned above, the number of sampled eddies as a function of the eddy type (propagating or stationary CEs, and AEs) varies from one to four. For each type, eddies exhibit relatively similar characteristics, so we illustrate each eddy type by looking at a specific eddy. The typical AE structure is illustrated from mission #2 (AE2), the PCE in the southern basin from mission #4 (PCE4), and the SCE in the northern basin from mission #9 (SCE9).

3.1.1. AE

The selected eddy (AE2) has been observed during the glider mission #2 that took place from February to July 2008, and coincided with La Niña conditions, suitable for the generation of AEs (Table 1, Figure 5). About six eddies (four AEs, and two PCEs) have been detected from altimetry in the whole of the Solomon Sea during this glider mission. AE2 crossed the glider track on 12 March 2008. It was generated in the southeast Solomon Sea and drifted quite slowly during its short lifespan of 30 days. It can be seen along the glider track in the 100–300 km range (Figure 2). Altimetry and glider provide similar characteristics with an eddy diameter of ~200 km, and an eddy amplitude of 4–5 cm. The anticyclonic eddy velocity extends from the surface to 200 m depth, but the downward displacement of isotherms/isohalines is visible down to 300 m depth. The associated temperature (salinity) anomalies reach 1.4°C (0.1 psu) in the 100–280 m depth

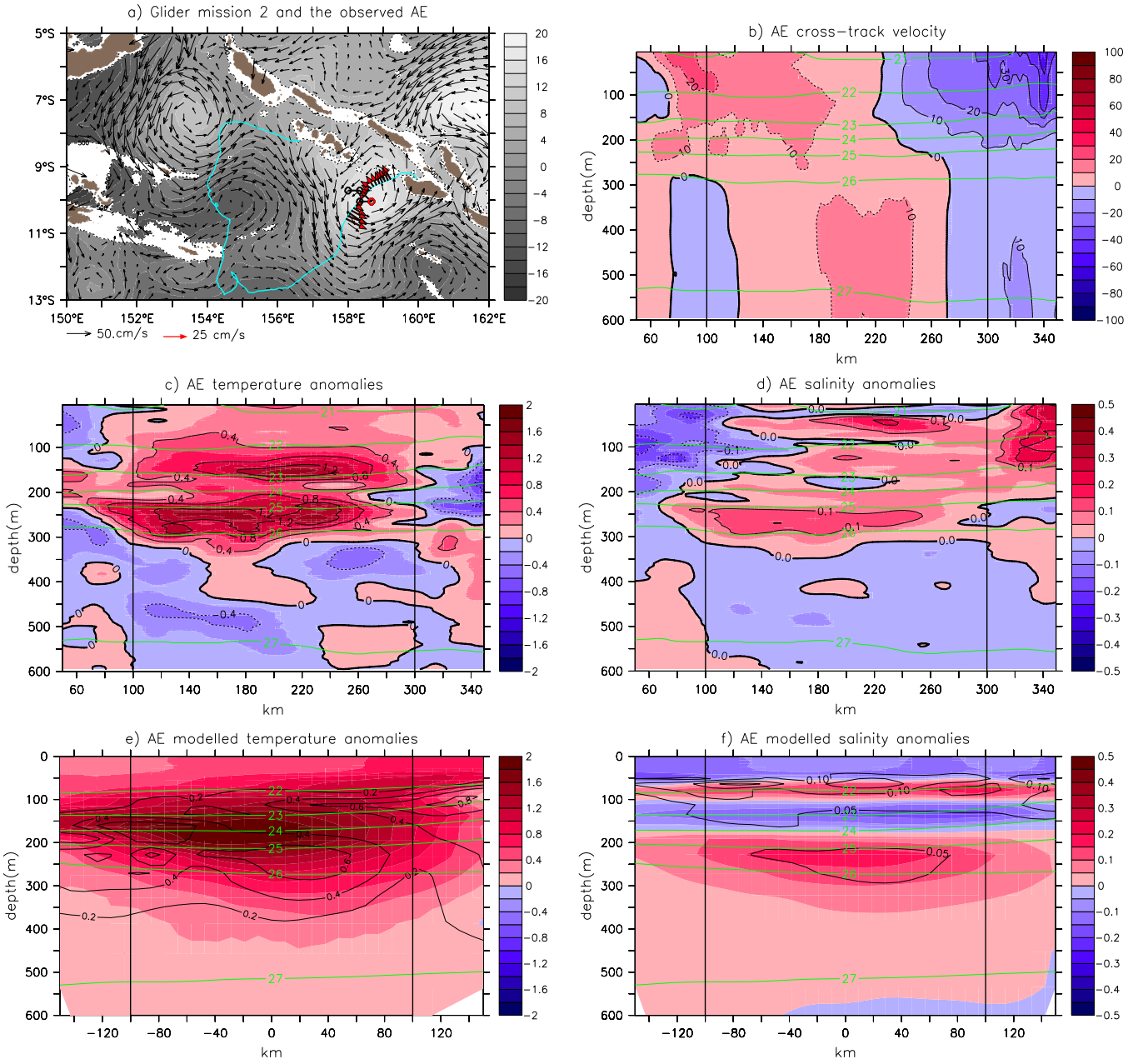


Figure 5. Signature of the anticyclonic eddy AE2 observed by the glider along its track during mission 2. (a) The dot line is the trajectory of AE2 detected on the altimetric maps, and the red dot is the location of AE2 when it has been sampled by the glider. Grey shading and black arrows show the altimetric SSH field (cm) and the corresponding geostrophic velocity field, respectively, on 12 March 2008 when A2 was sampled. The glider track is in cyan whereas the red arrows correspond to the absolute cross-track geostrophic velocity in the surface layer computed from the glider data. (b) Vertical section of the glider cross-track absolute geostrophic velocity (cm s^{-1}) across A2. (c) and (d) Vertical section of temperature (°C) and salinity anomalies, respectively. (e) and (f) are the composite signatures of modeled AEs for temperature (°C), and salinity, respectively (see text for details). The composite structures are in shading, and the corresponding standard deviation is in black contours. Density (kg m^{-3}) are in green contours. The black vertical lines delineate the eddy.

range (in the 22–26 kg m^{-3} sigma density range), and it results in lighter water within the eddy (see isopycnal levels in Figures 5c and 5d). The salinity signature should reflect the downward displacement of the subsurface salinity maximum with positive/negative anomaly below/above the mean salinity maximum. The positive anomaly is clearly evidenced whereas the negative anomaly is less marked. The surrounding waters have very contrasting salinity signatures, and eddy isopycnal mixing of salty waters could be particularly efficient as discussed in section 4.2 to reduce the signature of isopycnal heaving induced by downwelling vortices.

3.1.2. Propagating CE

The selected propagating cyclonic eddy (PCE4) has been observed during the glider mission #4 that took place between November 2008 and February 2009, and coincided with neutral ENSO conditions (Table 1, Figure 6). During this mission, Six eddies have been detected by altimetry. The PCE4 was generated in the southeast Solomon Sea, and during its lifespan of 56 days, it propagated westward before vanishing in the central Solomon Sea. In both the altimetry and glider data, the diameter and the amplitude of the eddy are of 160 km and 3.6 cm, respectively. The cyclonic eddy velocity extends from the surface to 250 m depth, and is maximum at the surface. It induces an upward displacement of isopycnals up to 20 m. The associated temperature anomaly reaches −1°C in the 150–270 m depth range ($\sigma = 24$ – 26.2 kg m^{-3}). The salinity anomaly reaches +0.2 in the upper thermocline and −0.1 psu below, reflecting the upward displacement of the subsurface salinity maximum and the underlying water mass. From the lower surface water (50 m, $\sigma = 22$ kg m^{-3}) to the midthermocline depth (270 m, $\sigma = 26.2$ kg m^{-3}), the combined effect of temperature

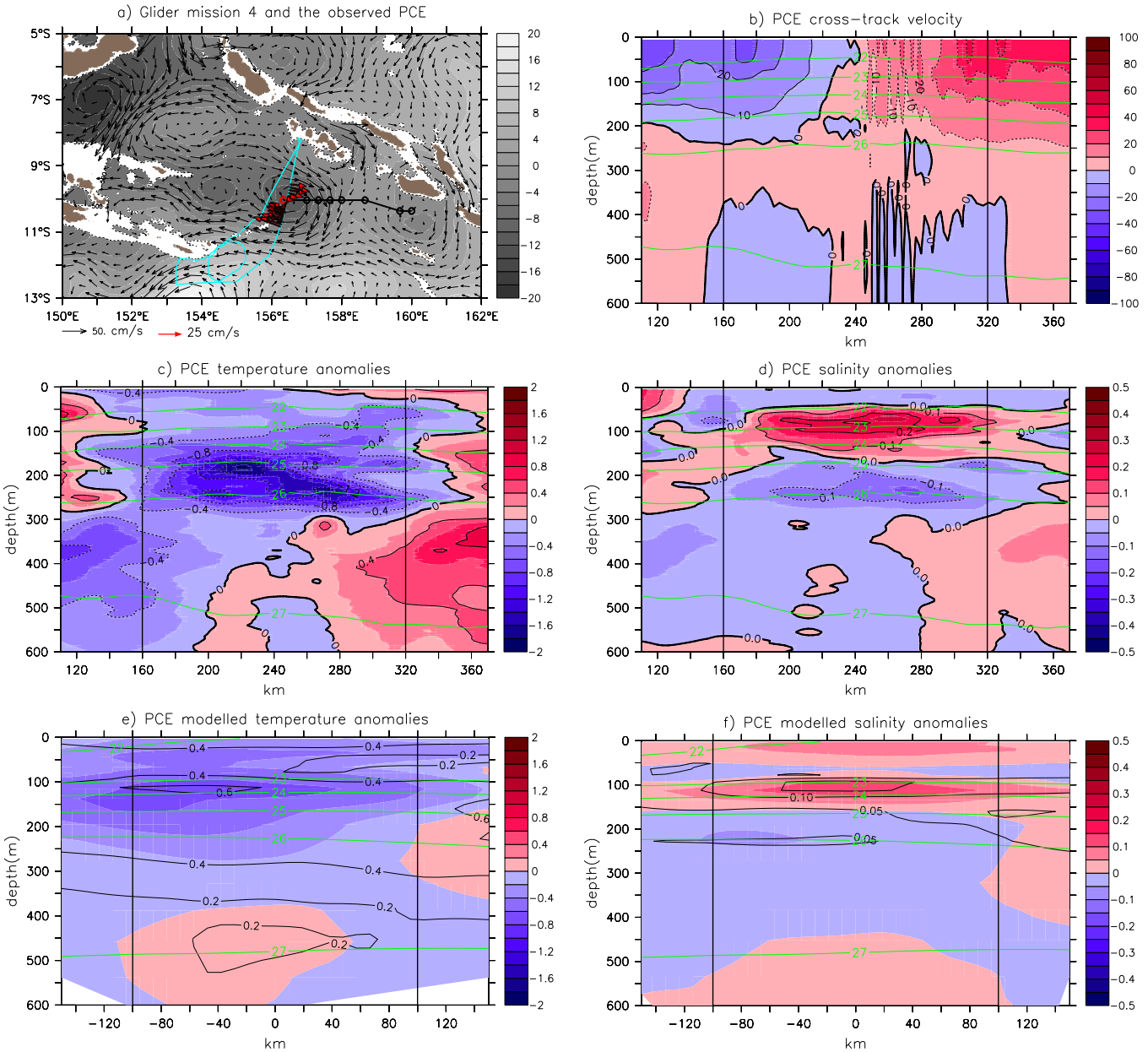


Figure 6. Same as Figure 5 for the propagating cyclonic eddy PCE4 of mission #4.

and salinity anomalies induce denser water in the eddy core than in the surroundings (see isopycnal levels in Figures 6c and 6d).

3.1.3. Stationary CE

The selected stationary cyclonic eddy (SCE9) was observed during the glider mission #9 that took place over the April to September 2010 period coinciding with neutral ENSO conditions (Table 1, Figure 7). It is the only mission that sampled the northern Solomon Sea. During this mission, eight eddies were detected from altimetry, and among them three SCEs spanning 75% of the considered period. During its journey on the northern basin the glider sampled on 15 July 2010 an intense cyclonic eddy just south of New Britain which had a lifespan of 21 days. The eddy diameter was of ∼200 km and its amplitude of 11.6 cm in the glider data against 8.2 cm on altimetry. The upwelling of relatively deep and cold water is evidenced by the vertical isopycnal displacement of more than 50 m in the near-surface layers (Figures 7b–7d), associated with the dipole in salinity corresponding to the uplift of the salinity maximum. Noted the fresh waters eddy

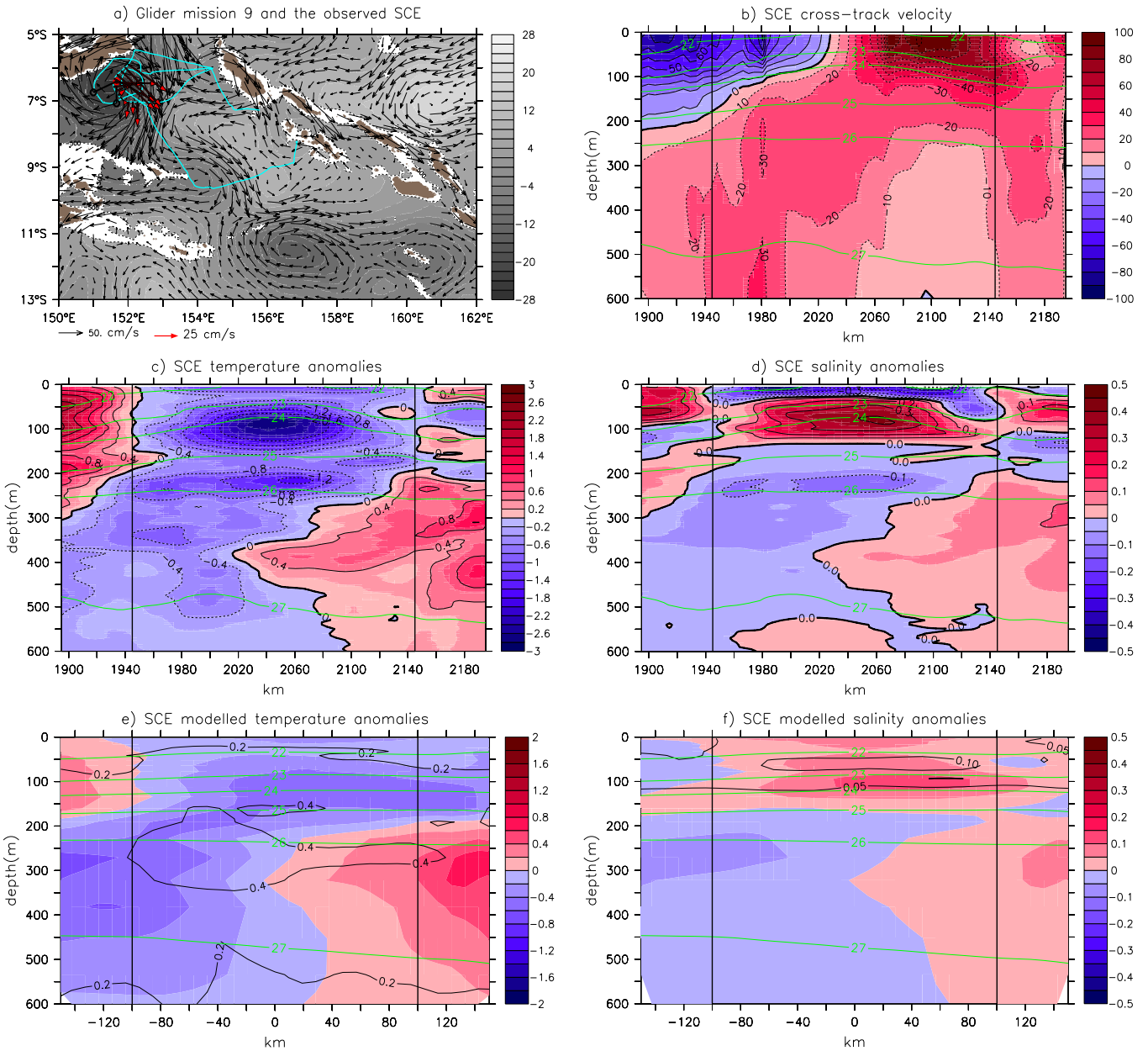


Figure 7. Same as Figure 5 for the stationary cyclonic eddy SCE9 of mission #9.

signature at the surface that would require more information to investigate the role of air-sea interactions. The cyclonic swirl velocity was maximum at the surface reaching more than 80 cm s^{-1}, and its vertical extension is limited to the top 200 m depth. Temperature and salinity anomalies are maximum at 100 m depth reaching −2.4°C and +0.4 psu, respectively. They induce denser water in the eddy core than in the surroundings from the surface to the thermocline depth (250 m depth, $\sigma = 26$ kg m^{-3}) (not shown).

In summary, based on this specific sample, the different eddy types have relatively similar characteristics. The observed eddies have radii of 80–100 km, but recall that the size of eddies is constrained by the use of altimetry where only large eddies can be detected. Their velocity is maximum at the surface and decrease down to 150–200 m depth. The associated temperature and salinity anomalies extend deeper down to 250–300 m depth. These anomalies are significant, reaching maximum values of ±2°C in temperature and ±0.2 psu in salinity, and are probably mainly related to the vertical displacement of the upper thermocline waters ($\sigma = 23 - 26$ kg m^{-1} σ).

3.2. Eddy Vertical Structure as Simulated From the Model

The aim of this section is to compare the observed vertical structure of the eddies with the modeled ones detected at similar locations. We do not expect that observed and modeled eddies can be collocated in time and space, because eddy generation by instabilities makes their occurrence stochastic (in addition, the two data sets do not cover the same period). However, 4 simulated eddies were identified near the location of AE2, 13 near the location of PCE4, and 15 near the location of SCE9. Similarly, to the eddies sampled by gliders, we investigate the signatures of the modeled eddies along the corresponding glider tracks. From the model, we computed eddy anomalies relative to a reference field rather than using the "differential anomaly." Classically, authors reference eddy anomalies to a climatological field (e.g., Chaigneau et al., 2011). In the Solomon Sea, seasonal and interannual variability are strong enough to induce temperature and salinity variations of the same order than eddy effects. Therefore, eddy temperature and salinity anomalies were computed relative to low-pass filtered fields (half-power at 7 months). The obtained anomalies were not strongly different from the ones estimated from the former method.

As for the glider data, simulated eddies corresponding to a specific eddy type have relatively similar characteristics. Their sizes and their velocity profiles along the glider track are similar (not shown). Because they are more numerous than eddies sampled by gliders, we construct composites for each eddy type by averaging their properties. Modeled eddy temperature and salinity mean anomalies and their corresponding standard deviation are presented on Figures 5−7e and 7f for AE, PCE, and SCE, respectively. The comparison between a model mean and observations of individual eddies is not straightforward, and the discrepancies between glider observations and model composites are mainly explained by the diversity of individual eddy vertical structures. This is clearly shown by the standard deviation of the eddy composite which is as high as its mean and centered at the location corresponding to the anomaly maximum. Some specific modeled eddies exhibit similar signature than the eddy sampled by the glider. It is however, more meaningful to show the signature of a composite eddy rather than of a specific eddy matching the observations. For AE, values of temperature and salinity anomaly are in the same range for both the model and observations (Figure 5). They correspond to the same sigma density range ($\sigma = 22 - 26$ kg m^{-3}) but there is a difference in depth of 20–30 m that illustrates a slight model bias. The negative salinity anomaly around the 23 sigma level, that reflects the downward displacement of SPTW, is less pronounced in the glider data. The positive salinity anomaly at the 22 sigma level is interpreted as eddy mixing at the level of the mixed layer depths as discussed in section 4.2. For PCE, temperature and salinity anomalies are smaller than observed but the associated variability is of same order (0.6°C/0.15 psu) meaning that some modeled eddies are as strong as the sampled one (Figure 6). Anomalies stretch from the 22 to the 26 sigma levels. It is noticeable that the 22 sigma level in the composite eddy outcrops at the surface whereas it is at 50 m depth in the glider data. Same comments hold for SCE (Figure 7), but in that case the eddy observed by the glider is particularly energetic with the effect of strong upward isopycnal displacement with an outcropping of the 22 sigma level not present in the composite eddy. If the difference between PCEs and SCEs is clearly evidenced in the observation, modeled composites of PCEs and SCEs are essentially identical, leading to the conclusion that PCEs and SCEs, though different by their propagations and location, exhibit the same vertical structures. Differences seen between both types of CEs by glider sampling are explained by the diversity of individual eddies, also found in the model.

At this stage we have few in situ observations of eddies observed along glider tracks. Their characteristics compare relatively well with eddies simulated in the model. In the following, an overall description of Solomon Sea eddies based on the model simulation is achieved in order to get information on their role for the Solomon Sea circulation.

4. Eddy Impacts on Solomon Sea Circulation

Thanks to glider data, we have a refined description of some of Solomon Sea eddies. Taking advantage of the synergy between data and model, we further analyze from the model their potential to generate T, S anomalies, and to modify water masses. We first need to define an "automatic" procedure to characterize modeled eddies in their 3-dimensions. The following discussion is focused exclusively on model results.

4.1. Modeled 3-D Eddies and Their Trapping Depths

Eddies are first detected at the surface using the closed contour method with SSH providing their amplitudes and equivalent radius (e.g., section 2.4). To extend eddy information on the vertical, we use the Q parameter that represents the second invariant of the velocity gradient tensor (Kurian et al., 2011). According to Isern-Fontanet et al. (2003), it can be expressed in the following form for planar flows:

$$Q = -\left(\frac{\partial u}{\partial x}\right)^2 - \left(\frac{\partial v}{\partial x}\right)\left(\frac{\partial u}{\partial y}\right), \tag{2}$$

where u and v are eastward and northward velocities. A similar expression can be derived from Okubo-Weiss parameter taking into account the normal and shear components of the strain and the relative vorticity of the flow (Kurian et al., 2011). The two terms on the right-hand side of equation (2) account for deformation and rotation, respectively. Hence, eddy cores can be identified at every vertical level by connected regions (i.e., closed contour) where rotation strongly dominates deformation, e.g., $Q > Q_0$, with $Q_0 = 0.5 \times 10^{-9}$ s^{-2} being a positive threshold value chosen by trial and error. A complete discussion on eddy characteristics discussed below can be found in Chelton et al. (2011). At the surface, the closed contours of SSH and Q compare relatively well. At depth, the definition of the eddy scale is based on the contour within the eddy interior that has the maximum averaged speed (the swirl velocity of the eddy). This contour of maximum swirl velocity corresponds approximately to a contour of zero relative vorticity, and the estimation of the eddy radius based on this criterion tends to be smaller than an estimate based on SSH or Q (Chelton et al., 2011). The advective nonlinearity parameter (NL) is defined as the ratio U/c, where *U* is the swirl velocity and *c* is the translation speed of the eddy estimated at each point along the eddy trajectory. NL > 1 implies nonlinear eddies: the speed of rotation exceeds the speed of propagation and eddies can effectively "trap" and transport water properties along their tracks (Chaigneau et al., 2009; Chelton et al., 2011; Kurian et al., 2011). The nonlinearity parameter, computed at every vertical level, gives information on the vertical extent of the trapped fluid. An example of the Q parameter, the eddy scale, and the depth of trapped fluid is shown in Figure 8. It shows an AE with a clear signature in terms of Q parameter with a maximum value at 80 m depth just below the mixed layer depth. Its scale is of ~150 km, and its trapping depth extends until 200 m depth over the Surface Waters (SW, $\sigma < 23.3$ kg m^{-3}) and the Upper Thermocline Waters (UTW, 23.3 kg m^{-3} $< \sigma <$ 25.7 kg m^{-3}).

The different parameters are estimated for each modeled eddy. For the different eddy types, the nonlinear parameter as a function of

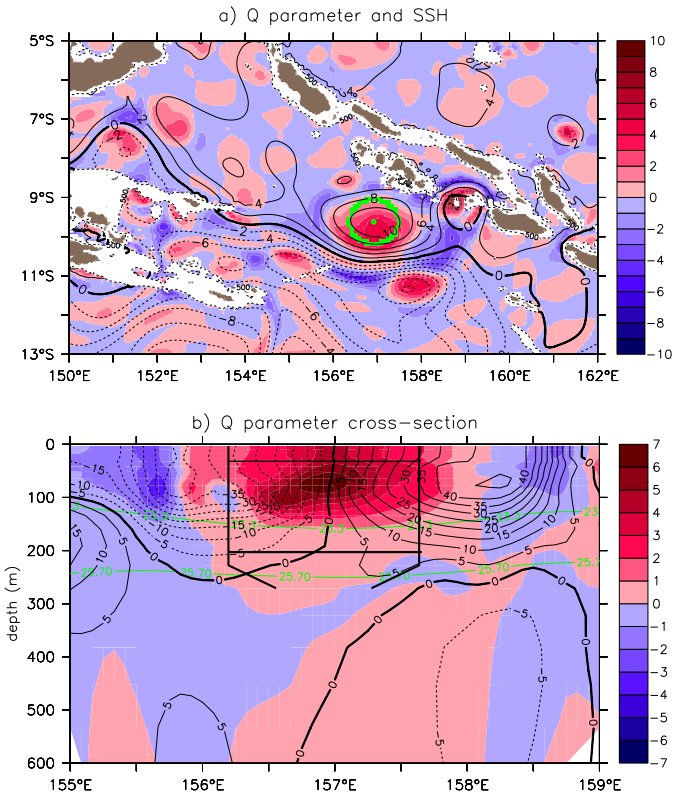


Figure 8. (a) Horizontal distribution of the Q parameter (shading, 10^{-9} s^{-2}) estimated from the model exhibiting an AE centered at 156.9°E, 9.6°S (green point). The green circle delineates the eddy radius. Superimposed in contour is the SSH field. (b) Depth/longitude section of the Q parameter (shading, 10^{-9} s^{-2}) at the location of AE. The thick black lines delineate its horizontal extension function of depth defined by the max swirl velocity and its vertical extension from the NL parameter defined to 1. The thin black line locates the mixed layer depth. The velocity section (cm s^{-1}) is in black contours, and the density (kg m^{-3}) of SW and UTW are in green contours.

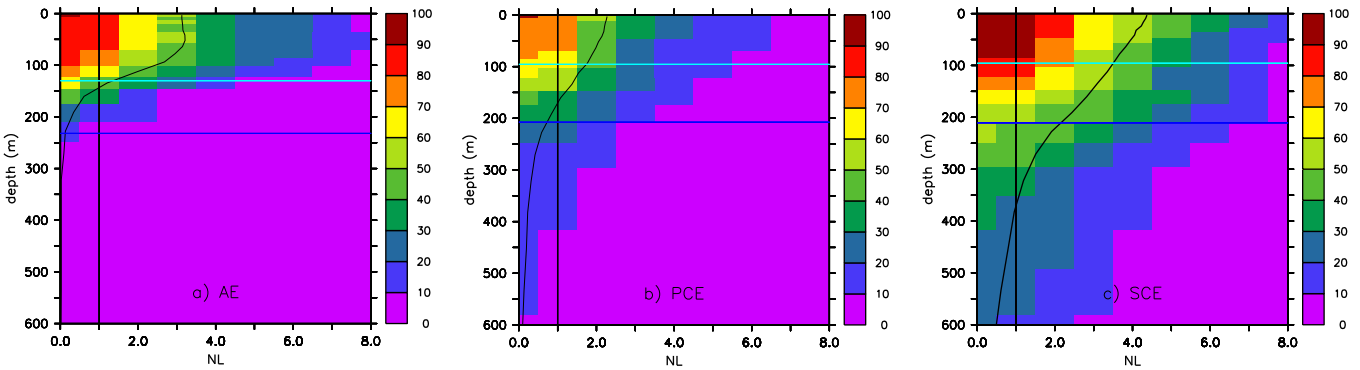


Figure 9. (a) Vertical profile of the nonlinear parameter (NL) averaged for all AEs (Thick black line). In shading is the periodogram of NL showing the distribution of cumulative number of eddies from high to small NL in percentage of the total number of eddies. The thin vertical line is for NL = 1. The cyan (blue) horizontal lines are for the 23.3 (25.7) sigma level that define SW (UTW), respectively. (b) Same as Figure 9a for PCEs and (c) same as Figure 9a for SCEs.

depth is shown in Figure 9. Their histograms are represented in terms of percentage of cumulated eddies for every vertical level. For example, 50% of AEs have a nonlinear parameter greater than or equal to 2 at 100 m depth and 20% of AEs have a nonlinear parameter greater than or equal to 6 at 50 m depth.

Most of the eddies are nonlinear (NL > 1) but there are some notable differences between the different eddy types. For AEs, the trapped fluid is mainly located in the Surface Waters (SW), in the first 140 m depth layer, and 40% of AEs have a nonlinear parameter greater than or equal to 3 at 100 m depth (Figure 9a). SCEs appear to be more efficient to trap waters (Figure 9c). About 60% of SCEs have a nonlinear parameter greater than or equal to 3 at 100 m depth. Their signature may extend deeply under the surface with 30% of SCEs having a nonlinear parameter greater than 3 at 300 m depth. However, SCE cannot really transport water masses and impact tracers' budget because they are relatively stationary. The scenario is quite different for PCEs. Because they are less energetic and propagate faster, their nonlinear parameter is relatively weak (Figure 9b). Less than 20% of PCEs have a nonlinear parameter greater than or equal to 3 at 100 m depth. Even if some PCEs may extend well deeper than 140 m, the nonlinear parameter is close to one questioning their efficiency to effectively transport water masses. Based on a 60% criterion of occurrence, the depth of trapped waters may be estimated to 130 m for AEs, 90 m for PCEs, and 160 m for SCEs.

4.2. Impact of Eddies on Modeled Water Masses

Eddy temperature and salinity anomalies are discussed both as a function of depth and of density. As a function of depth, they illustrate mainly the vertical displacement of the water column. As a function of density, they reflect mainly either isopycnal transport or diapycnal mixing. Most of eddy characteristics discussed above and below are summarized in Table 2.

4.2.1. Eddy Temperature and Salinity Anomalies as a Function of Depth

With regard to the temperature and salinity profiles (see Figure 2 for an example), it is expected that vertical displacements of the water column induced by an eddy result in temperature anomalies at the thermocline level, and salinity anomalies of opposite sign located below and above the salinity maximum of SPTW (as described in section 3). Based on the modeled eddy data set, we quantify eddy anomalies as a function of depth, and of the different water masses. For each eddy, temperature and salinity anomalies are computed as described in section 3.2, and they are averaged at each vertical level. Their mean vertical profiles are presented for each eddy type (propagating or stationary CEs, and AEs) on Figure 10. Temperature anomalies are maximum at the interface between SW and UTW, and extend to the core of the UTW. Temperature anomalies reach 1.1°C at 160 m for AEs, −0.9°C at 130 m depth for PCEs, and −0.8°C at 110 m depth for SCEs (Table 2). For the three eddy types, salinity anomalies show extrema values (positive for PCE and SCE and negative for AEs) at the interface between SW and UTW and at the base of the UTW (negative for PCE and SCE and positive for AEs). The depth

Table 2
Mean Geometrical Properties (Radius and Depth of Trapped Fluid), Amplitude, and Maximum Temperature, Salinity, and Density Anomalies at the Corresponding Depth (Ta/m, Sa/m, σa/m, *Respectively) for Each Modeled Eddy Type (AEs, PCEs, SCEs)*

	AEs	PCEs	SCEs
Radius (km)	90	80	80
Depth (m)	130	90	160
Amplitude (cm)	4. ± 2	6.5 ± 3	5 ± 2
Ta/depth (°C/m)	1.1 ± 0.5/160	−0.9 ± 0.6/130	−0.8 ± 0.7/110
Sa/depth (psu/m)	−0.1 ± 0.1/110	0.14 ± 0.1/90	0.15 ± 0.2/80
σa/depth (kg m^{-3}/m)	−0.4 ± 0.2/130	0.4 ± 0.3/90	0.4 ± 0.3/90

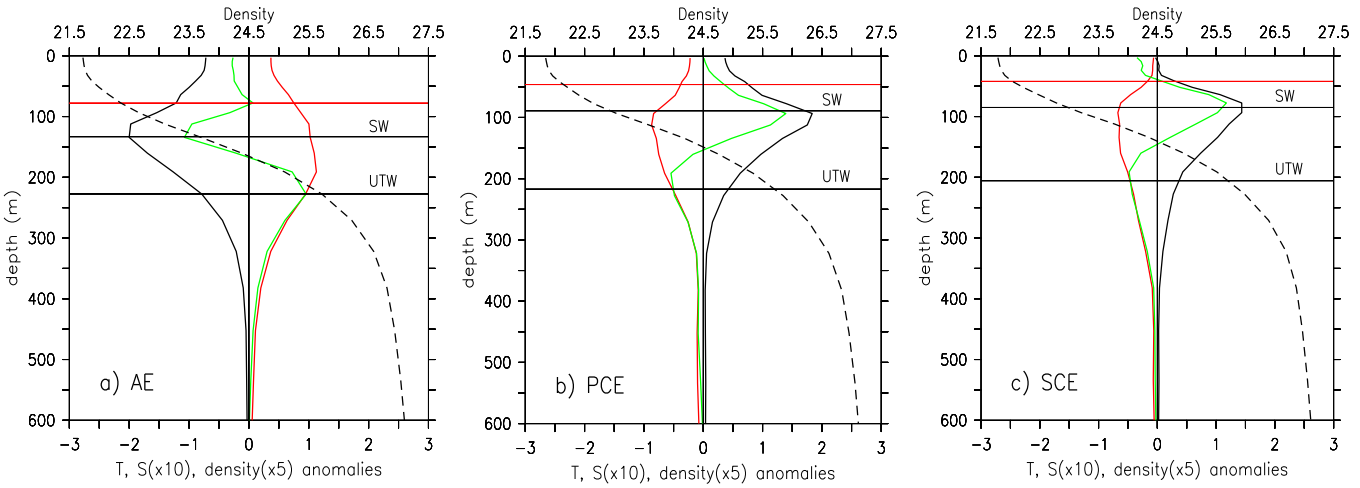


Figure 10. Mean temperature (red, °C), salinity (green, psu), and density (thick black, kg m^{-3}) anomalies within eddies as a function of depth for (a) AEs, (b) PCEs, and (c) SCEs. The corresponding mean density profile of the reference fields (i.e., section 3.2) is shown as a dashed line. Horizontal black lines delineate the Surface Water (SW) and Upper Thermocline Water (UTW). The red line indicates the mixed layer depth. The *x* axis on top is for density (kg m^{-3}) whereas *x* axis on bottom is for anomalies of temperature, Salinity (×10), and density (×5).

separation between these two extrema depends mainly on the SW depth that varies from 130 m for AEs to 80–90 m for CEs (Figure 10). For AEs, salinity anomalies reach −0.1 psu (+0.09 psu), at 110 m (230 m) depth. For PCEs, salinity anomalies reach +0.14 psu (–0.05 psu) at 90 m (190 m) depth, and for SCEs, +0.15 psu (−0.06 psu) at 80 m (190 m) depth (Table 2). In terms of density, the eddy signatures are well visible with negative (positive) density anomalies from the surface down to 400 (∼300) m depth for AEs (CEs). In fact, eddy signatures depend on the strong tropical stratification with a well-marked pycnocline in the 100–300 m depth range, and maximum of density anomalies are observed at the base of the SW. Above this level, eddies tend to be strongly nonlinear meaning that the observed anomalies could be advected by propagating eddies.

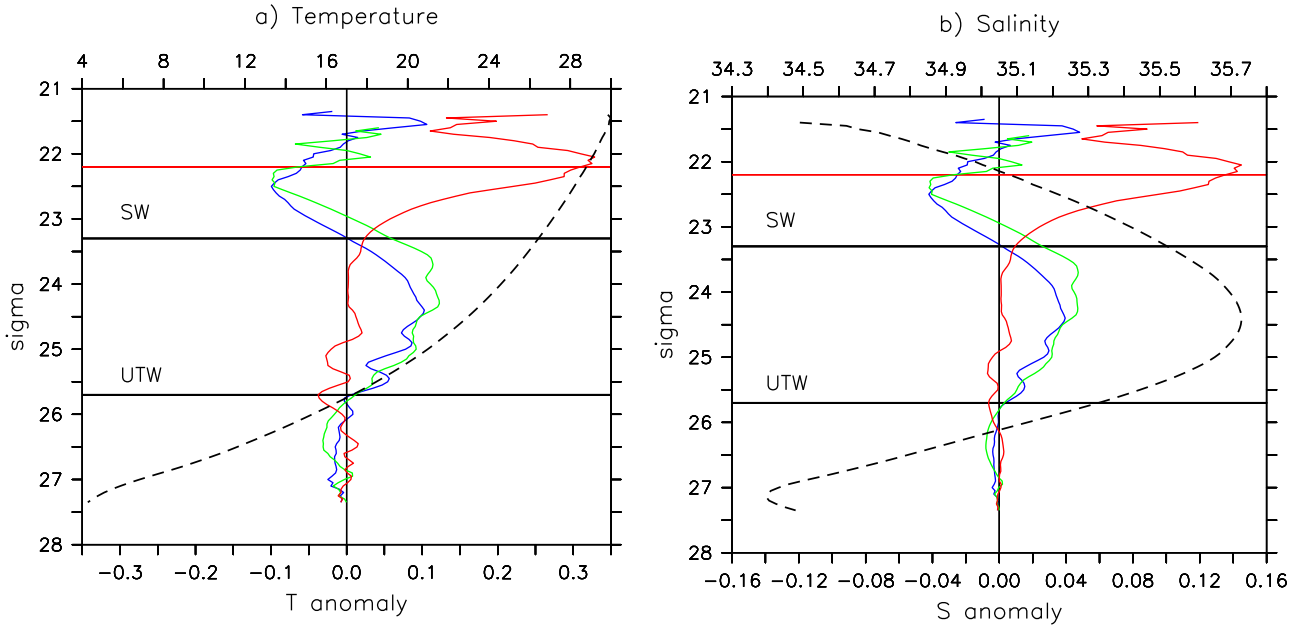


Figure 11. (a) Temperature (°C) and (b) salinity anomalies as a function of sigma levels for AEs (red), PCEs (blue), and SCEs (green). The thick-dashed line shows the mean (a) temperature and (b) salinity profile in the Solomon Sea. Horizontal black lines delineate the two main water masses: Surface Water (SW) and Upper Thermocline Water (UTW). The horizontal red line indicates the mean density at the mixed layer depth.

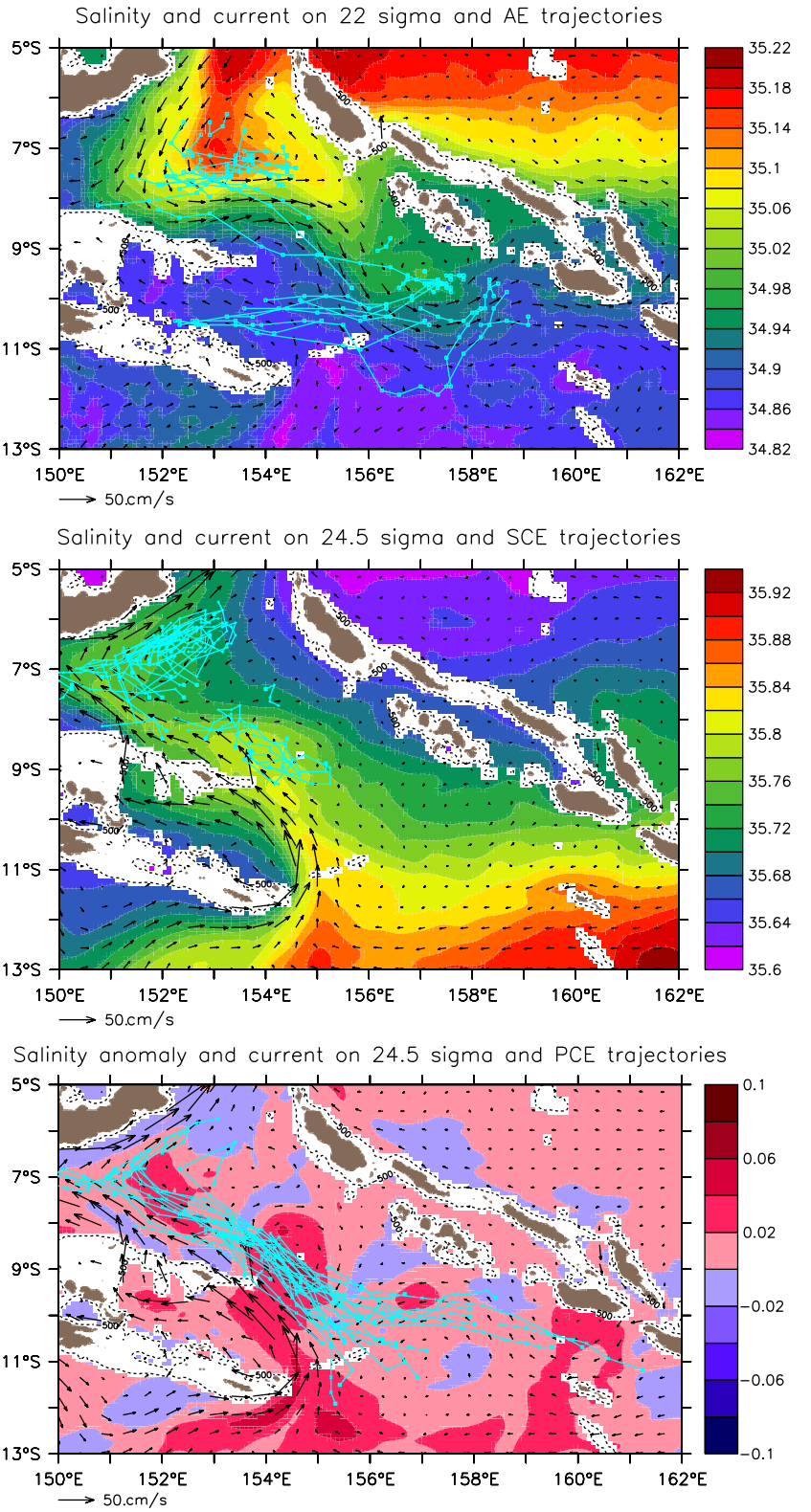


Figure 12. (a) Salinity and current fields at the 22 sigma level density averaged over the time where AEs are present. AEs trajectories are superimposed in light blue. (b) Salinity and current fields at the 24.5 sigma level density averaged over the time where SCEs are present. SCEs trajectories are superimposed in light blue. (c) Salinity anomaly (relative to the reference low-frequency field) and current fields at the 24.5 sigma level density averaged over the time where PCEs are present. PCEs trajectories are superimposed in light blue.

4.2.2. Eddy Temperature and Salinity Eddy Anomalies as a Function of Density

In addition to inducing temperature and salinity anomalies with depth, it is worth looking at possible effects of eddies on water mass transformation. Eddy and reference fields are projected on a vertical density coordinate, and temperature and salinity eddy anomalies are computed as a function of density. They are presented for each eddy type on Figure 11. For AEs, temperature/salinity anomalies are localized in SW with an extreme on the 22 sigma density level with values of 0.35°C and 0.15 psu, respectively. If AEs anomalies are significant, CEs anomalies have lower magnitude of 0.1°C and 0.04 psu. For CEs, temperature/salinity anomalies exist both in SW and UTW with opposite sign. Negative anomalies in SW are centered at the 22.5 sigma density level and positive anomalies in UTW correspond with the salinity maximum of SPTW centered on the 24.5 sigma density level.

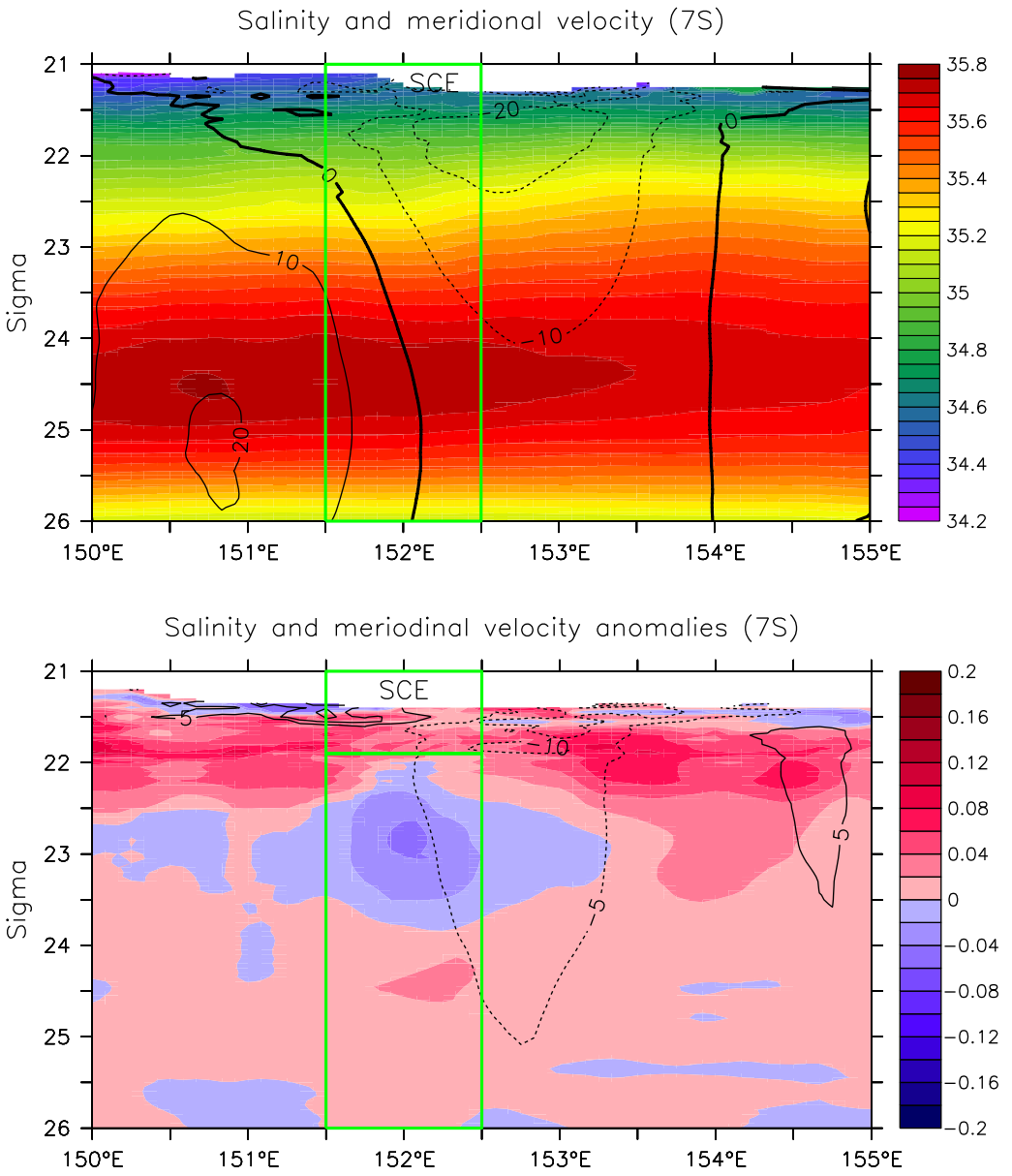


Figure 13. (a) Longitude/sigma density section at 7°S of salinity (psu, shading) and meridional velocity (cm s^{-1}, contour) averaged over the time where SCEs are present. (b) Same as Figure 13a but for salinity and meridional velocity anomalies relative to the reference low-frequency field. The green lines delineate the mean position and mixed layer sigma density level of SCEs.

Figure 12a shows the mean salinity and currents at the 22 sigma level in the whole area, averaged at times when AEs are present. In agreement with Gourdeau et al. (2014), mean oceanic conditions corresponding to AEs generation are characterized with a stronger SSI, and an intrusion of warmer and saltier waters through the Solomon Strait. When AEs are detected, the whole Solomon Sea is warmer and saltier, and AEs composites are thus associated with saltier/warmer SW waters. A deepening of the mixed layer depth (defined by a temperature change from the ocean surface of 0.5°C) from 76 m for the reference fields to 88 m for AEs is also observed inside eddies. AEs trap this water mass, and have the potential to transport it when propagating across the Solomon Sea.

SCEs are part of the mean circulation in the northern Solomon Sea, characterized by cyclonic recirculation located at 7°S and 9°S (Figure 12b) (e.g., Figure 1b in Gourdeau et al., 2014). Therefore, they cannot transport water masses, so eddy anomalies must be at first order the result of eddy dynamics. A density/longitude section of salinity anomalies at 7°S gives evidence of the eddy signature (Figure 13). On the western side (151°E) of the section, the SPTW salinity maximum is advected by the NGCU (Figure 13a), then it turns east along the New Britain coast. Part of the NGCU recirculates southward at around 152°–154°E, forming a cyclonic rotation that is accentuated during SCEs generation. SCEs are characterized by anomalies inside the eddy contrasting with the surrounding waters with fresher/cooler SW waters just below the mixed layer depth defined with the 22 sigma density level (Figure 13b). The upwelled high salinity could be eroded by diapycnal mixing with the lower salinity at the base of the mixed layer depth, resulting in a lower salinity in the 22–23.5 sigma level, and exported toward deeper layers as suggested by the weak increase in salinity around the depth of the salinity maximum. This salinity anomaly may also correspond to advection of higher salinity in the recirculation.

PCEs have a similar signature in temperature and salinity anomalies on isopycnals than the SCEs, with fresher/cooler SW waters, and the same explanations could hold. They travel over long distance from the southeastern to the northwestern Solomon Sea. They are first advected westward by a branch of the NVJ entering the Solomon Sea at its southeastern boundary before being advected northward by the NGCU. Their trajectories follow the eastern flank of the NGCU and the SPTW salinity maximum characterized by significant positive anomalies since its entrance in the Solomon Sea (Figure 12c). Based on the NL parameter (Figure 9b), more than 50% of PCEs could be able to transport the SPTW waters and the corresponding salinity anomaly. It suggests that isopycnal transport by PCEs could play a role in transporting the saltier/warmer UTW waters.

To summarize, AEs, by trapping warmer and saltier SW waters, could play a role on mixed layer characteristics and in return, on local air-sea interaction. For CEs, interaction of the upwelling with mixed layer dynamics through diapycnal mixing could explain downward vertical fluxes between SW and UTW, and for PCEs, isopycnal transport could be efficient to transport salt/warm SPTW anomalies.

5. Conclusions

In this paper, we further explored the issue of mesoscale activity in a low-latitude region, the Solomon Sea, which is an exemplary situation of eddy activities in a low-latitude western boundary current. Contrary to the ocean midlatitudes, the evidence, as well as the role, of mesoscales have been relatively little studied to date. The first synoptical explorations of the Solomon Sea have been made with numerical models, suggesting a high level of mesoscale activity (Djath et al., 2014a; Hristova et al., 2014). This was further explored in conjunction with altimetric observations (Gourdeau et al., 2014). Since 2007, the routine glider transects bring a lot of new data and complementary information (Davis et al., 2012). The objective of this paper was to make a synergistic approach using model outputs, altimetric data, and glider observations. It is of much interest indeed to take benefit of these complementarity sources of data, because:

1. gliders provide high-resolution data and have access to the vertical dimension, though only on specific tracks and for limited times;
2. gridded altimetry provides an information only at the surface, and has a limited horizontal resolution; and
3. numerical simulations are clearly more synoptic, especially in time and space but are limited by the model performances due to erroneous model parameterizations and imperfect forcing functions.

Therefore, the approach taken in this paper was first to use together glider and altimetry to identify some eddy features of particular relevance, and to assess the model performances and second to explore the characteristics of the modeled eddies to quantify their possible role in the Solomon Sea circulation and mixing. The size of eddies is constrained by the use of altimetry to detect them, and only relatively large (mesoscale, O (100 km)) eddies can be observed.

The main result of this work lies first in the description of eddies allowed with this multidata set approach. Most importantly, we found a quite good consistency between in situ data and model outputs which in many ways validates the modeled eddies and more generally give some reassurance of the model relevance, at least in the case of the Solomon Sea.

Three eddy types as defined in Gourdeau et al. (2014) are identified and discussed: anticyclonic eddies (AE), propagating anticyclonic eddies (PCE), and stationary anticyclonic eddies (SCE). All the three eddy types have been sampled by gliders at least once, and their descriptions are in agreement with the model results. Whatever the eddy types their signatures are well visible with relatively similar characteristics that can be summarized as follows. Their radii are of 80–100 km. Their velocities are maximum at the surface and decrease down to 150–200 m depth. Density anomalies extend from the surface down to 300 m depth and maximum of density anomalies are observed at the base of the SW. The associated temperature and salinity anomalies reach maximum values of ± 2°C in temperature and ± 0.2 psu in salinity, and are mainly related to the vertical displacement of surface and upper thermocline waters ($\sigma = 22 - 26$ kg m^{-3}). Temperature anomalies are maximum at the top of UTW (23.3 kg m$^{-3} < \sigma < 25.7$ kg m^{-3}), and extend to the core of the UTW whereas salinity anomalies have two extrema, one at the interface between SW ($\sigma < 23.3$ kg m^{-3}) and UTW and the another one at the base of UTW in relation with the vertical displacement of the SPTW salinity maximum. These surface-intensified characteristics are quite different from midlatitude regions, where eddies have been shown to extend to 1,000 m depth or deeper (Castelao, 2014; Chaigneau et al., 2011).

Beyond this joint analysis of all these data that has allowed to better characterize the specific features of cyclonic and anticyclonic eddies in the Solomon sea, we also tried to make emerge some overall first conclusions on their role on the regional circulation. In this regard, there are several results that are worthwhile to synthesize here. Most of the eddies are nonlinear meaning than eddies can trapped and transport water properties. But there are some significant differences between the different eddy types.

For AEs, the trapped fluid is mainly located in the Surface Waters (SW, sigma < 23.3 kg m^{-3}), in the first 140 m depth layer. AEs are mainly generated when the southward flow from SSI increases. AEs propagating westward could be particularly efficient to advect such saltier/warmer SW coming from the intrusion of equatorial Pacific waters at Solomon Strait. Isopycnal transport could explain water mass transformation along their pathway from the eastern Solomon Sea to the central/western Solomon Sea. It could impact the characteristics of the NGCC, and play a role on mixed layer characteristics and in return, on local air-sea interaction.

For CEs, the upwelled high salinity could be eroded by diapycnal mixing with the lower salinity at the base of the mixed layer depth. SCEs are mainly phased with the modulation of cyclonic mean circulation present in the northern Solomon Sea. Despite the fact that they appear to be efficient to trap waters, they cannot transport water masses and impact tracers' budget because they are relatively stationary. The scenario is quite different for PCEs. PCEs are mainly generated when the NVJ enters directly the Solomon Sea. PCEs are first advected westward by the NVJ before to be advected northward by the NGCU. This mean circulation during PCEs corresponds with saltier/warmer SPTW water entering the Solomon Sea and PCEs could be efficient to transport such SPTW anomalies.

Mesoscale activity is clearly modulated at seasonal and interannual time scale (Gourdeau et al., 2014). The importance of eddies to transport anomalies coming from the SSI or the NVJ is highly conditioned by large-scale conditions. During El Niño, the NVJ increases transporting cooler and fresher thermocline waters, whereas during La Niña, the SSI increases transporting warmer and saltier surface waters (Melet et al., 2012). So, the impact of eddies, and the respective role of AEs and CEs on Solomon Sea circulation depends on the background flow. Such relationship will be investigated in the future.

Our approach has clearly some limits. First, some limits rely on the data sets used including: limited synopticity and limited vertical extension for the gliders, insufficient horizontal resolution, inaccuracy, and surface

data only for altimetry, model performances, etc. Moreover, eddies under consideration must be large enough to be detected by altimetry as altimetry was used for identifying eddies of interest. Small eddies are therefore not taken into consideration whereas the 1/36° model clearly reveals that they are present and active (Djath et al., 2014a, Hristova et al., 2014). Perspectives for this work are to go further than an eddy description to really assess the role of mesoscale and associated submesoscale activity on the Solomon Sea circulation. Also, strong internal tides exist in the Solomon Sea, and an objective will be to analyze the respective effects of mesoscale activity and high-frequency motions using a 1/36° model including tides. The continuity of glider observational program is a key point. Also, we can expect more accuracy from the recent altimetric products that are more efficient in complex bathymetric area like the Solomon sea (i.e., with SARAL/AltiKa satellite) and even more in the future with the SWOT mission that will provide 2-D maps of dynamic topography over the satellite swaths.

Acknowledgments
This work is a contribution to the CLIVAR/SPICE international program. This research has been conducted with the support of the Centre National d'Etudes Spatiales (CNES/TOSCA), the Centre National de la Recherche Scientifique (CNRS/INSU LEFE), and the Institut de Recherche pour le Développement (IRD). The authors would like to thank the DRAKKAR team for providing them with the high-resolution global ocean simulation, and especially J. M. Molines for his availability. We thank R. Davis from Scripps for his involvement in repeated transects across the Solomon Sea from Spray underwater gliders conducted under the Consortium on the Ocean's Role in Climate (CORC) program on boundary current measurements. More information on these glider data (https://doi.org/10.21238/S8SPRAY2718) can be found at: http://spraydata.ucsd.edu/projects/Solomon. We also thank Yves Morel and Julien Jouanno from LEGOS for their helpful comments.

References

Adcroft, A., Hill, C., & Marshall, J. (1997). Representation of topography by shaved cells in a height coordinate ocean model. *Monthly Weather Review*, *125*, 2293–2315. https://doi.org/10.1175/1520-0493(1997)125<2293:ROTBSC>2.0.CO;2

Barnier, B., Madec, G., Penduff, T., Molines, J.-M., Treguier, A.-M., Le Sommer, J., . . . De Cuevas, B. (2006). Impact of partial steps and momentum advection schemes in a global ocean circulation model at eddy-permitting resolution. *Ocean Dynamics*, *56* (5–6), 543–567. https://doi.org/10.1007/s10236-006-0082-1

Castelao, R. M. (2014). Mesoscale eddies in the South Atlantic Bight and the Gulf Stream Recirculation region: Vertical structure. *Journal of Geophysical Research: Oceans*, *119*, 2048–2065. https://doi.org/10.1002/2014JC009796

Chaigneau, A., Eldin, G., & Dewitte, B. (2009). Eddy activity in the four major upwelling systems from satellite altimetry (1992–2007). *Progress in Oceanography*, *83*, 117–123. https://doi.org/10.1016/j.pocean.2009.07.012

Chaigneau, A., Gizolme, A., & Grados, C. (2008). Mesoscale eddies off Peru in altimeter records: Identification algorithms and eddy spatio-temporal patterns. *Progress in Oceanography*, *79*, 106–119. https://doi.org/10.1016/j.pocean.2008.10.013

Chaigneau, A., Le Texier, M., Eldin, G., Grados, C., & Pizarro, O. (2011). Vertical structure of mesoscale eddies in the eastern South Pacific Ocean: A composite analysis from altimetry and Argo profiling floats. *Journal of Geophysical Research*, *116*, C11025. https://doi.org/10.1029/2011JC007134

Chelton, D. B., Schlax, M. G., & Samelson, R. M. (2011). Global observations of nonlinear mesoscale eddies. *Progress in Oceanography*, *91*, 167–216. https://doi.org/10.1016/j.pocean.2011.01.002

Cravatte, S., Ganachaud, A., Duong, Q.-P., Kessler, W. S., Eldin, G., & Dutrieux, P. (2011). Observed circulation in the Solomon Sea from SADCP data. *Progress in Oceanography*, *88*, 116–130. https://doi.org/10.1016/j.pocean.2010.12.015

Davis, R. E., Kessler, W. S., & Sherman, J. T. (2012). Gliders measure western boundary current transport from the south pacific to the equator. *Journal of Physical Oceanography*, *42*, 2001–2013. https://doi.org/10.1175/JPO-D-12-022.1

Djath, B., Melet, A., Verron, J., Molines, J.-M., Barnier, B., Gourdeau, L., & Debreu, L. (2014b). A 1/36° model of the Solomon Sea embedded into a global ocean model: On the setting up of an interactive open boundary condition nested model system. *Journal of Operational Oceanography*, *7*(1), 34–46. https://doi.org/10.1080/1755876X.2014.11020151

Djath, B., Verron, J., Melet, A., Gourdeau, L., Barnier, B., & Molines, J.-M. (2014a). Multiscale analysis of dynamics from high resolution realistic model of the Solomon sea. *Journal of Geophysical Research: Oceans*, *119*, 6286–6304. https://doi.org/10.1002/2013JC009695

Ganachaud, A., Cravatte, S., Melet, A., Schiller, A., Holbrook, N. J., Sloyan, B. M., . . . Send, U. (2014). The Southwest Pacific Ocean circulation and climate experiment (SPICE). *Journal of Geophysical Research: Oceans*, *119*, 7660–7686. https://doi.org/10.1002/2013JC009678

Gasparin, F., Ganachaud, A., Maes, C., Marin, F., & Eldin, F. (2012). Oceanic transports through the Solomon Sea: The bend of the New Guinea coastal undercurrent. *Geophysical Research Letters*, *39*, L15608. https://doi.org/10.1029/2012GL052575

Gasparin, F., Maes, C., Sudre, J., Garcon, V., & Ganachaud, A. (2014). Water mass analysis of the Coral Sea through an Optimum Multiparameter method. *Journal of Geophysical Research: Oceans*, *119*. https:/doi.org/10.1002/2014JC010246

Germineaud, C., Ganachaud, A., Sprintall, J., Cravatte, S., Eldin, G., Alberty, M. S., & Privat, E. (2016). Pathways and water mass properties of the thermocline and intermediate waters in the Solomon Sea. *Journal of Physical Oceanography*, *46*, 3031–3049. https://doi.org/10.1175/JPO-D-16-0107.1

Grenier, M., Cravatte, S., Blanke, B., Menkes, C., Koch-Larrouy, A., Durand, F., Melet, A., & Jeandel C. (2011), From the western boundary currents to the Pacific Equatorial Undercurrent: Modeled pathways and water mass evolutions. *J. Geophys. Res.*, *116*, C12044–a, doi: 10.1029/2011JC007477.

Grenier, M., Jeandel, C., Lacan, F., Vance, D., Venchiarutti, C., Cros, A., & Cravatte, S. (2013). From the subtropics to the central equatorial pacific ocean: Neodymium isotopic composition and rare earth element concentration variations. *Journal of Geophysical Research: Oceans*, *118*, 592–618. https://doi.org/10.1029/2012JC008239

Gourdeau, L., Kessler, W. S., Davis, R. E., Sherman, J., Maes, C., & Kestenare, E. (2008). Zonal jets entering the coral sea. *Journal of Physical Oceanography*, *38*(3), 715–725. https://doi.org/10.1175/2007JPO3780.1

Gourdeau, L., Verron, J., Melet, A., Kessler, W., Marin, F., & Djath, B. (2014). Exploring the mesoscale activity in the Solomon sea: A complementary approach with a numerical model and altimetric data. *Journal of Geophysical Research: Oceans*, *119*, 2290–2311. https://doi.org/10.1002/2013JC009614

Hristova, H. G., & Kessler, W. S. (2012). Surface circulation in the Solomon Sea derived from Lagrangian drifter observations. *Journal of Physical Oceanography*, *42*, 448–458. https://doi.org/10.1175/JPO-D-11-099.1

Hristova, H. G., Kessler, W. S., McWilliams, J. C., & Molemaker, M. J. (2014). Mesoscale variability and its seasonality in the Solomon and Coral Seas. *Journal of Geophysical Research: Oceans*, *119*, 4669–4687. https://doi.org/10.1002/2013JC009741

Isern-Fontanet, J., García-Ladona, E., & Font, J. (2003). Identification of marine eddies from altimetric maps. *Journal of Atmospheric and Oceanic Technology*, *20*(5), 772–778. https://doi.org/10.1175/1520-0426(2003)20<772:IOMEFA>2.0.CO;2

Kurian, J., Colas, F., Capet, X., McWilliams, J. C., & Chelton, D. B. (2011). Eddy properties in the California current system. *Journal of Geophysical Research*, *116*, C08027. https://doi.org/10.1029/2010JC006895

Large, W., & Yeager, S. (2004). Diurnal to decadal global forcing for ocean and sea-ice models: The data sets and Flux climatologies. In *Climate and global dynamics division* (Tech. Note NCAR/TN-4601STR). Boulder, CO: The National Center for Atmospheric Research. https://doi.org/10.5065/D6KK98Q6

Large, W., & Yeager, S. (2009). The global climatology of an interannually varying air-sea flux data set. *Climate Dynamics*, *33*, 341–364. https://doi.org/10.1007/s00382-008-0441-3

Lecointre, A., Molines, J.-M., & Barnier, B. (2011). *Definition of the interannual experiment ORCA12.L46-MAL95, 1989–2007* (Internal Rep. MEOM-LEGI-CNRS, LEGI-DRA-21-10-2011, 25 p.). Grenoble, France: Drakkar.

Levitus, S., Boyer, T. P., Conkright, M. E., O'Brien, T., Antonov, J., Stephens, C., . . . Gelfeld, R. (1998). *NOAA Atlas NESDIS 18,World Ocean Database 1998: VOLUME 1: Introduction* (346 pp.). Washington, DC: U.S. Gov. Printing Office.

Madec, G., & the NEMO team. (2008). *NEMO ocean engine*. France: Note du Pôle de modélisation, Institut Pierre-Simon Laplace (IPSL).

Melet, A., Gourdeau, L., Kessler, W. S., Verron, J., & Molines, J.-M. (2010a). Thermocline circulation in the Solomon sea: A modeling study. *Journal of Physical Oceanography*, *40*(6), 1302–1319. https://doi.org/10.1175/2009JPO4264.1

Melet, A., Gourdeau, L., & Verron, J. (2010b). Variability in Solomon sea circulation derived from altimeter sea level data. *Ocean Dynamics*, *60*(4), 883–900. https://doi.org/10.1007/s10236-010-0302-6

Melet, A., Gourdeau, L., Verron, J., & Djath, B. (2012). Solomon Sea circulation and water mass modifications: Response at ENSO timescales. *Ocean Dynamics*, *63*, 1–19. https://doi.org/10.1007/s10236-012-0582-0

Melet, A., Verron, J., Gourdeau, L., & Koch-Larrouy, A. (2011). Solomon Sea water masses pathways to the Equator and their transformations. *Journal of Physical Oceanography*, *41*, 810–826. https://doi.org/10.1175/2010JPO4559.1

Penduff, T., Le Sommer, J., Barnier, B., Treguier, A.-M., Molines, J.-M., & Madec, G. (2007). Influence of numerical schemes on current-topography interactions in 1/4° global ocean simulations. *Ocean Science*, *3*, 509–524. https://doi.org/10.5194/os-3–509-2007

Pietri, A., Echevin, V., Testor, P., Chaigneau, A., Mortier, L., Grados, C., & Albert, A. (2014). Impact of a coastal- trapped wave on the near-coastal circulation of the Peru upwelling system from glider data. *Journal of Geophysical Research: Oceans*, *119*, 2109–2120. https://doi.org/10.1002/2013JC009270

Qin, X., Sen Gupta, A., & van Sebille, E. (2015). Variability in the origins and pathways of Pacific Equatorial Undercurrent water. *Journal of Geophysical Research: Oceans*, *120*, 3113–3128. https://doi.org/10.1002/2014JC010549

Rio, M. H., Guinehut, S., & Larnicol, G. (2011). New CNES-CLS09 global mean dynamic topography computed from the combination of GRACE data, altimetry, and in situ measurements. *Journal of Geophysical Research*, *116*, C07018. https://doi.org/10.1029/2010JC006505

Sherman, J., Davis, R. E., Owens, W. B., & Valdes, J. (2001). The autonomous underwater glider "Spray". *IEEE Journal of Oceanic Engineering*, *26*, 437–446. https://doi.org/10.1109/48.972076

Simpson, J. J., Dickey, T. D., & Koblinsky, C. J. (1984). An offshore eddy in the California current system. Part I: Interior dynamics. *Progress in Oceanography*, *13*, 5–49. https://doi.org/10.1016/0079-6611(84)90004-1

Verron, J., & Blayo, E. (1996). The no-slip boundary condition and the Gulf Stream separation problem. *Journal of Physical Oceanography*, *26*(9), 1938–1951. https://doi.org/10.1175/1520-0485(1996)026 < 1938:TNSCAS>2.0.CO;2